Machining temperature comparative analysis of end mill and novel tool in orbital drilling of CFRP composite

Linghao Kong
Harbin Institute of Technology
Dong Gao
Harbin Institute of Technology
Yong Lu (luyhit@163.com)
Harbin Institute of Technology

Research Article

Keywords: Orbital drilling, Machining temperature, CFRP; Cutting tool, Temperature distribute model.

Posted Date: April 5th, 2021

DOI: https://doi.org/10.21203/rs.3.rs-181521/v1

Machining temperature comparative analysis of end mill and novel tool in orbital drilling of CFRP composite

1) Linghao Kong E-mail: linghao8959@163.com
School of Mechatronics Engineering, Harbin Institute of Technology, Harbin, China
2) Dong Gao E-mail: gaodong@hit.edu.cn
School of Mechatronics Engineering, Harbin Institute of Technology, Harbin, China
3) Yong Lu E-mail: luyong@hit.edu.cn
School of Mechatronics Engineering, Harbin Institute of Technology, Harbin, China

Abstract

Applying Carbon fiber-reinforced plastics (CFRPs) instead of traditional materials can improve the structural strength and reduce the weight of the spacecraft. However, the defects and the rejections still impede the wide application of CFRP for the contrasting thermo-mechanical properties of fibers and resin. A lower machining temperature can reduce burrs and delamination effectively. To study the cutting temperature of orbital drilling in CFRP, the processing temperature of the conventional orbital drilling (COD) was compared with the novel orbital drilling and reaming tool (ODR), and a heat transfer model considering the influence of convective heat transfer on cutting temperature was also proposed in this research, which can explain the reason of the novel tool with a lower cutting temperature. On the basis of the analysis of the kinematic mechanisms, a cutting force prediction model for the process of orbital drilling was presented. The three-dimensional, unsteady state, nonhomogeneous partial differential heat transfer equation in polar coordinates was established, and solved with the finite difference approach. The results show that the predictions of models are coincided to the experimental data, and ODR tool can reduce the processing temperature of orbital drilling effectively.

Keywords: Orbital drilling; Machining temperature; CFRP; Cutting tool; Temperature distribute model.

Funding: National Key Research and Development Program of China under Grant No. 2019YFB1704803

Conflicts of interest: We declare that we do not have any commercial or associative interest that represents a conflict of interest in connection with the work submitted.

Availability of data and material: All data are fully available without restriction.

Code availability: Not applicable

Authors' contributions: LHK, YL, and DG conceived and designed the study. LHK performed the experiments. LHK wrote the paper. LHK, YL and DG reviewed and

edited the manuscript. All authors read and approved the manuscript.

Nomenclature

a_p	Screw pitch of helical path
e	Eccentric of helical path
d	Diameter of milling part
f_t	Feed rate in tangential
f_z	Feed rate in z direction
D	Diameter of peripheral cutting edges
F	Cutting force of the ODR tool
F_M	Cutting force generated by milling part
F_R	Cutting force generated by reaming part
F_P	Cutting force generated by peripheral cutting edges
n_t	Spindle rotation speed
n_h	Orbital rotation speed
K_{Mac} K_{Mae}	Force coefficients related to the milling part
r_t	Radius of milling part
θ_t	Angular positions of the tool coordinates to the workpiece coordinate
θ_0	Initial angle position of tool coordinate
ω_h	Angular velocity of orbital rotation
φ_{e1}	Angle position of the 1st cutting edge
φ_0	Initial angle position of the 1st cutting edge
N	Number of cutting edges on the tool
ω	Angular velocity of spindle rotation
φ_e	Angle between two adjacent cutting edges
j	The j th cutting edge on the tool
φ_{ej}	Angle position of the j th cutting edge
$\varphi_j(t,z)$	Angle position of the j th cutting edge with the height of z at the time of t
ds	The length of a cutting element

dz	The height of a cutting element
z	The height of the cutting edge element
β	The helix angle of the end mill
$h_j(\varphi_i, z)$	Thickness of chip at the angle of φ_j the height of z
H	Height of reaming part
R_z	Radius of reaming part at the height of z
dF_{xj}^{tR}, dF_{yj}^{tR}, dF_{zj}^{tR}	The cutting force in x, y and z direction of a cutting edge element on the Reaming part in the cutter coordinate
$F_{xj}^{tR}, F_{yj}^{tR}, F_{zj}^{tR}$	The cutting force in x, y and z direction, of the reaming part in the cutter coordinate
$F_{xj}^{tP}, F_{yj}^{tP}, F_{zj}^{tP}$	The cutting force in x, y and z direction, of the peripheral cutting edges in the cutter coordinate
F_x^t, F_y^t, F_z^t	The cutting force of the ODR tool in the x, y and z direction in tool coordinate
F_x^w, F_y^w, F_z^w	The cutting force of the ODR tool in the x, y and z direction in workpiece coordinate
$\dot{Q}_{fs}(\varphi)$	The heat generated on the shear plane in first deformation zone of a cutting element
F_s	The shearing force of a cutting element
v_s	Shear velocity
$\dot{Q}_{fsw}$	The heat $\dot{Q}_{fs}(\varphi)$ transfer to the workpiece
K_w	Thermal diffusivity of workpiece
ϕ_n	Shear angle
γ_n	Front rake angle
$\dot{Q}_{tf}(\varphi)$	The heat generated due to the friction in third deformation zone of a cutting element
$F_f(\varphi)$	The force of friction of a cutting element
$\dot{Q}_{tfw}$	The heat $\dot{Q}_{tf}(\varphi)$ transfer to the workpiece
b	Cutting width
l_{wf}	Length of furrow area
$\lambda_1, \lambda_2, \lambda_2$	Heat conductivity of CFRP in x,y,z direction
r_w, θ_w, z_w	Represent the radius, angle and height of the node's position
T	Temperature of the workpiece

T_0	Ambient temperature
ρ	Density of workpiece
c	Heat capacity of workpiece
h	Convective heat transfer coefficient
$q(r,\theta,z,t)$	Heat flux generated of the heat source

1 Introduction

With excellent mechanical and physical properties such as high strength and light weight, carbon fiber-reinforced plastic (CFRP) has been widely applied in aviation and aerospace. As structural components and skins, a substantial number of rivets and bolts with high dimensional tolerance and surface quality need to be drilled in the CFRP parts [1] for connecting. However, unsatisfactory machining quality still restricts the reliability of CFRP parts. CFRP is a laminated structure generally composed of carbon fiber cloth and resin. Carbon fiber has high strength and high temperature resistance, while the resin is sensitive to temperature, the elasticity modulus and strength will plummet when its temperature exceeds the glass transition temperature(150-250℃)[2]. CFRP workpiece has low thermal conductivity and specific heat capacity, the heat accumulation phenomena during machining leads to an apparent temperature rise around the processing area. The insufficient interlaminar shear strength and transverse tensile strength of CFRP will be more prominent with the impact of processing temperature[3]. Many severe machining defects will be generated due to this deficiency, such as burring and fuzzing, fibers pull out, matrix cracking and delamination. In particular, delamination is judged to be the most catastrophe defect, in that it leads to rapid declines in stiffness and carrying capacity of the mechanical components. Thus, the study of the magnitude and distribution of CFRP workpiece temperatures during processing should be of great significance.

To improve the drilling quality of CFRP components, the effects of tool performance and cutting parameters on the damage of CFRP hole making have been widely studied in the past decades. The effects of the drill types (twist drill[4-6], candlestick drill[6,7], step drill[8,9], core drill[10,11], etc.), tool geometry(diameter[12,13], point angle[14] and chisel length[15]) and tool material[15,16] on the machining quality were studied. Although the drill bit with special structures could achieve superior processing quality, sometimes high quality, high efficiency, low cost and other industry requirements are still difficult to satisfy. Orbital drilling[17,18], wobble milling[19,20], vibration-assisted cutting[21], water jet cutting[22], laser cutting[23] and EDM[24] are also used to improve the drilling quality of CFRP component. Among the methods mentioned, orbital drilling has been widely adopted in practice. In this method, the end mill rotates around the tool axis which is paralleled to the hole axis, at the same time making planetary motion around the hole axis[25]. Orbital drilling has many advantages over traditional drilling, a longer tool life, a lower cutting temperature and a less thrust force

that contributes to reduce the possibility of delamination effectively [17,26]. Based on the comprehensive consideration of machining quality, cost and efficiency, orbital drilling is supposed to be the most promising machining method for CFRP drilling. To further improve the quality of orbital drilling, tilted helical milling[25], tilted orbital grinding[1], two-step technique[27] are also proposed.

To clarify the temperature field inside the workpiece and the tool, the mechanisms of heat generation and heat distribution in the cutting process have been studied for a long time. Cutting temperature in metal cutting was studied as early as 1907, and Taylor[28] revealed the effect of cutting speed on cutting temperature and tool life. In the early researches on cutting temperature, data were obtained mainly by experimental measurements, such as thermocouples, infrared imagery, and thermo-colors. The experimental measurement is non-reusable, time-consuming and costly. Therefore, the numerical and analytical models are proposed, which have been widely concerned and used up to now. Based on the moving heat source model in the 1940s, the prototype of the model of cutting temperature was basically established. After years of researches, the analytical model has the ability to predict the magnitude and distribution of workpiece temperatures and has been applied to many engineering fields. In order to predict the cutting temperature more accurately, Komanduri[29-31] studied the heat generated in shear plane and tool-chip interface in the cutting process, and calculated the temperature field distribution at tool-chip interface. Berliner[32] proposed an analytical model which takes the cooling by means of a solution of a Fourier equation and the heat generated by three cutting deformation zones in account comprehensively, the theoretical results show a good predictive effect. By discretizing the cutting edge and the time history into micro-elements, the tool movement was simplified, then a model was established by Sen [33] to predict the cutting temperature of the workpiece during the end milling process which took consideration of the wear of flank face. The accuracy of the model is higher than that of the analytical model, and the prediction efficiency is higher than that of the finite element method, which can be used to optimize the cutting parameters. On the basis of the heat source method, Zhang[34] presented an analytical model for predicting the temperature distribution of coated cutting tools rake face, and the influences of parameters such as the friction coefficient of coated tool/workpiece on the temperature distribution of coated tool is also discussed. In the research of the magnitude and distribution of workpiece temperature, Richardson[35] pointed out that the increase of the cutting speed or feed rate can reduce the heat that transmitted into the workpiece. Based on the non-uniform heat distribution ratio along the interface of the primary and the second heat source, Huang[36] proposed a new model for analyzing cutting temperature, which improved the match and the predicting accuracy. With the development of calculation methods and the improvement of calculation capacity, finite element method (FEM) has been widely used in the calculation of cutting temperature[37-39]. FEM is time-consuming and the accuracy of the material's constitutive properties has a significant influence on the accuracy of the prediction. In the 1960s, Dutt[40] solved the differential heat transfer equations with the finite difference method and obtained an excellent prediction effect. With the enhancement of the computing power of computers, the finite difference method can be

used to solve the differential equation with high efficiency and accuracy. Lazoglu [41] presented a numerical model that predict the temperature fields in tool and chip in a time varying milling process. Jie [42,43] solved a three-dimensional heat transfer model describing the temperature field of the workpiece during helical milling by the Green function approach. Zhang [44] took a large number of exit temperature of CFRP drilling obtained by experimental measurement as the training object and established the prediction model of CFRP drilling exit temperature by neural network.

Cutting temperatures in machining significantly impact the tool life, size and shape tolerances and residual stress of the machined part. Several scholars have also studied the approach for reducing cutting temperature. Through the application of semi-artificial thermocouple, Sun [45] found that the cutting temperature showed a similar upward trend with the increase of cutting parameters. In order to optimize the tool life, Sheng [46] proposed a modeling coupling equation of cutting parameters based on optimal cutting temperature. Using RSM, Shah [47] studied the effects of cutting parameters and tool nose radius on the cutting temperature and the cutting force. Wang [48] studied the relationship between cutting parameters, cutting temperature and cutting force in CFRP milling with RSM, and pointed out that cutting speed has a significant influence on the cutting temperature. Ha [49] found the cutting temperature increase with the increasing of cutting speed on CFRP in high-speed machining, and resulted in the chips deforming from powder to spalling. Rajesh [50] established the regression equation about the influence of cutting parameters on cutting temperature and surface roughness and optimized it with a genetic algorithm to select the optimal cutting parameters. The research of the cutting temperature in drilling thermo plastic polymers by Weinert [51] showed that low cutting speed and high feeds are helpful to realize favored tool temperature and to reduce heat impact zone. Guimaraes[52] improved the thermal conductivity of the tool by incorporating copper heat sinks in a designated position of the tool. Behera [53] found that coated tools reduce cutting force and cutting temperature to a large extent in dry machining of Inconel 825 compared to uncoated tools. Sasahara [54] studied the effect of MQL on cutting temperature in driven rotary cutting, the result shows that the rotation of the tool and MQL can reduce the cutting temperature and decrease tool wear. Song [55] developed a combined nozzle that ejects MQL and cryogenic gas simultaneously to reduce Ti alloys' milling temperature and extend tool life. It can be seen that most of the researches on reducing the temperature of the machining area focus on the optimization of cutting parameters, the using of improved tools and the using of coolant.

CFRP materials are far less widely used than metal, most of the researches on the cutting heat of CFRP remain in experimental measurement methods, such as thermocouple[2], infrared imagery[44,56,57], fiber Bragg grating[58]. The processing temperature has an important influence on the quality of CFRP drilling. However, the using of the conventional cutting compound has an effect on the strength of CFRP workpiece, while the usage of cryogenic gas for cooling causes powdery chips floating in the air, posing a threat to the environment and operators' health. Therefore, researches on the temperature field distribution of CFRP workpiece during processing and the way to

reduce the processing temperature are scarcely reported.

Orbital drilling is considered to be the most promising method of CFRP drilling. In the previous study, utilizing the dedicated tool in orbital drilling, orbital drilling and reaming (ODR)[59] can further improve the processing quality, prolong the tool life, and reduce the processing temperature without changing the processing equipment of orbital drilling, which has a good prospect for application. To further study the machining performance of end mill and ODR tool, a numerical model revealing the magnitude and distribution of workpiece temperatures, which considered the influence of convective heat transfer on cutting temperature was proposed in this paper. Taking the different thermal diffusivity of CFRP in different directions into account, a three-dimensional, unsteady state, nonhomogeneous partial differential heat transfer equation in polar coordinates was established. And the finite difference approach was used to solve the heat transfer equation. The heat fluxes of two kinds of tools in processing were calculated. The temperature changes inside the workpiece of two kinds of cutting tools during machining were calculated and compared with the experimental results. The experiment results were in good agreement with the prediction model. This study verified that ODR tool in orbital drilling can reduce the cutting temperature in machining. Section 2 presents the process of machining temperature prediction. The experimental instruments and cutting parameters used in this research is recorded in section 3. The experimental results are analyzed in section 4, and the conclusion is drawn in the last section.

2Machining temperature of end mill and ODR tool in orbital drilling

2.1 Processing with ODR tool

Orbital drilling (helical milling) is a hole processing technique by eccentric milling with an end mill. Because of the planetary movement of the end mill, the part which is cutting at a low speed by the chisel edge on a twist drill is avoided totally, and the cutting force along the axis is decreased which reduce the possibility of delamination. With the influence of eccentricity, the drilled hole has a larger diameter than the tool, this forms a larger space to storage the chip, which improves the chip-removal and reduces tool-chip friction effectively. The intermittent cutting of peripheral cutting edge improves heat dissipation efficiency, reduces the tool temperature and the possibility of workpiece burns. ODR tool is used instead of the end mill in orbital drilling, the processing presents a novel material removal process which is different from conventional orbital drilling (COD). As can be observed in Fig.1, ODR tool consists of three parts, a milling part with a diameter of d, periphery cutting edges with a diameter of D, and a reaming part with a varied diameter which connects the periphery cutting edges to the milling part. The hole made by the milling part has a smaller diameter than the requirement. The reaming part is used for expanding the hole, which was made by

the milling part. Taking the material at exit as an example, the tool moves along the axis of the tool, the milling part of the ODR tool touches the bottom of the workpiece firstly, producing a hole with the diameter of d. On the impact of the combined effect of the spiral trajectory and the reaming part, the size of exit is expanded continuously, and the size is enlarged to the required size until the reaming part passed through the workpiece completely.

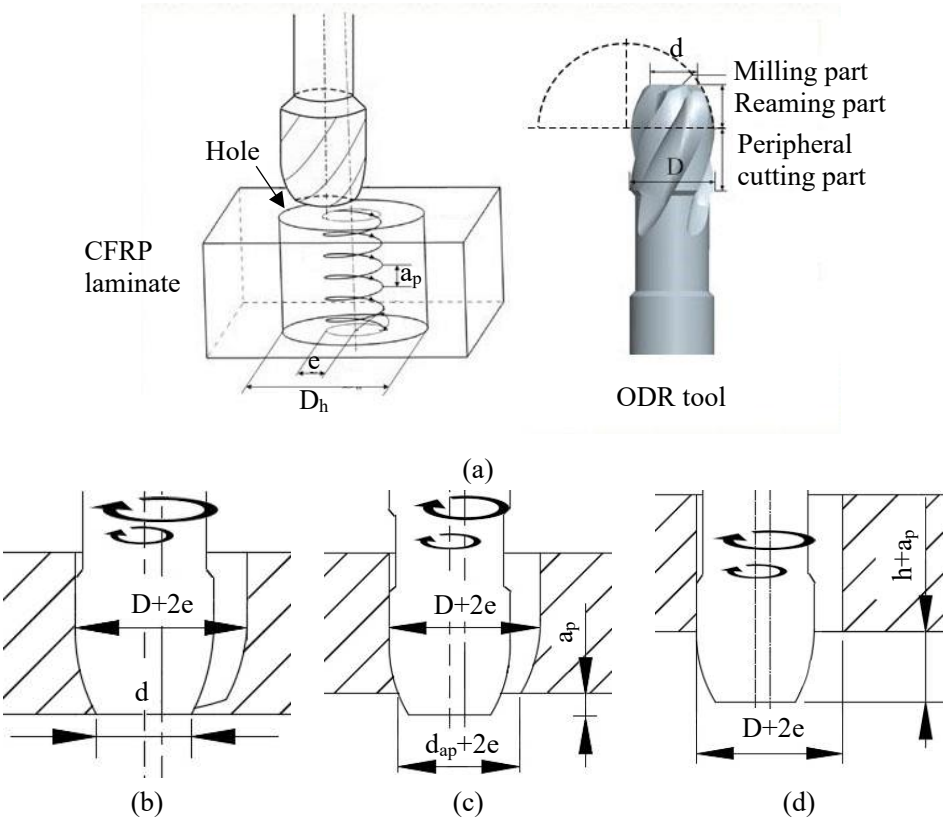

Fig. 1. ODR tool and the hole processing with ODR tool: (a) ODR tool, (b)-(d) exit formation of ODR tool

2.2 Temperature field prediction of the workpiece in processing

2.2.1 Analysis of cutting force in orbital drilling

To calculate the temperature distribution inside the workpiece, the cutting force model of orbital drilling should be established to calculate the heat generated in the cutting process at first. Owing to the shape of the ODR tool, the cutting force of ODR tool in orbital drilling is more complicated compared to the end mill. Therefore, this paper takes ODR tool as an example to model the cutting force of orbital drilling.

ODR tool is constituted of the milling part, the reaming part and the peripheral cutting edges, all of them will participate in cutting during the machining. Therefore, the model includes the influence of three parts on the cutting force, and the cutting force can be formulated as,

$$F(t) = F_M(t) + F_R(t) + F_P(t) \tag{1}$$

The spindle rotation speed n_t is far greater than the orbital rotation speed n_h in orbital drilling. Therefore, the influence of milling part due to the orbital rotation on the cutting force is ignored. Assuming that the milling part only produces the cutting force along the tool axis, which can be expressed by cutting force coefficient, cutting width and chip thickness as,

$$F_M = \left(K_{Mac} h_{za} + K_{Mae}\right) r_t \tag{2}$$

The modeling process of reaming part and peripheral cutting edges is similar, so illustrate by the reaming part as an example. The cutter coordinate $O_t X_t Y_t Z_t$ is established with the center of milling part as the origin, and the workpiece coordinate $O_w X_w Y_w Z_w$ is established with the center of the hole as the origin. The position of the tool and the cutting edge is shown as Fig.2 (a), and can be calculated by formula (7).

$$\theta_t(t) = \theta_0 + \omega_h t \tag{3}$$

$$\varphi_{e1} = \varphi_0 + \omega t \tag{4}$$

$$\varphi_e = 2\pi / N \tag{5}$$

$$\varphi_{ej} = \varphi_{e1} + (j-1)\varphi_e \tag{6}$$

$$\varphi_j(t, z) = \varphi_{ej} + \frac{z \cdot \tan\beta}{R} \tag{7}$$

The undeformed chip geometry in orbital drilling with ODR tool is shown in Fig.2 (b, c). The tool contains N cutting edges. Dividing the cutting edge j of reaming part into many tiny cutting edges, each element has a height of dz, and a length of ds.

$$ds = dz / \cos\beta \tag{8}$$

Taking the cutting edge element as the origin, the movement direction of the element as the Y axis, the direction pointing to the tool axis as the X axis, and the vertical direction as the Z axis to establish the elements coordinate. Then the tangential force (dF_{tj}), the radial force (dF_{rj}) and the axial force (dF_{aj}) of each cutting edge element can be expressed as,

$$\begin{cases} dF_{tj} = K_{tc} h_j\left(\varphi_j, z\right) dz + K_{te} ds \\ dF_{rj} = K_{rc} h_j\left(\varphi_j, z\right) dz + K_{re} ds \\ dF_{aj} = K_{ac} h_j\left(\varphi_j, z\right) dz + K_{ae} ds \end{cases} \tag{9}$$

Where φ_j is the instantaneous immersion angle of the cutting edge element, $h_j\left(\varphi_j, z\right)$ is the thickness of chip at the angle of φ_j the height of z, and K_{tc}, K_{te}, K_{rc}, K_{re}, K_{ac}, K_{ae} are the cutting force coefficients calibrated by experiments. As illustrated in Fig.2 (d), the edges move df along the y axis in the tool coordinate, the thickness of undeformed chip is related to angle position of the cutting edge element. Then the $h_j\left(\varphi_j, z\right)$ can be calculated as formula (10).

$$h_j\left(\varphi_j, z\right) = \sqrt{\left(R_z \cdot \sin\varphi_j + df\right)^2 + \left(R_z \cdot \cos\varphi_j\right)^2} - R_z \tag{10}$$

As the Fig.2 b and c shows, the edges cut into the workpiece at φ_{st}, and cut out at φ_{ex}, then the function $g\left(\varphi_j\right)$ is established to estimate whether the cutting element involves the processing.

$$g\left(\varphi_j\right) = \begin{cases} 1 & \varphi_{st} \le \varphi_j \le \varphi_{ex} \\ 0 & \varphi_j < \varphi_{st} \ or \ \varphi_{ex} < \varphi_j \end{cases} \tag{11}$$

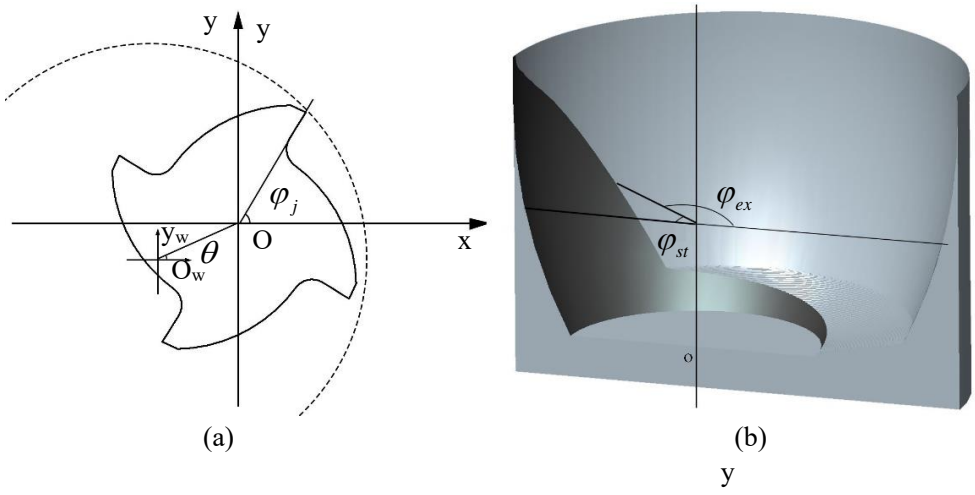

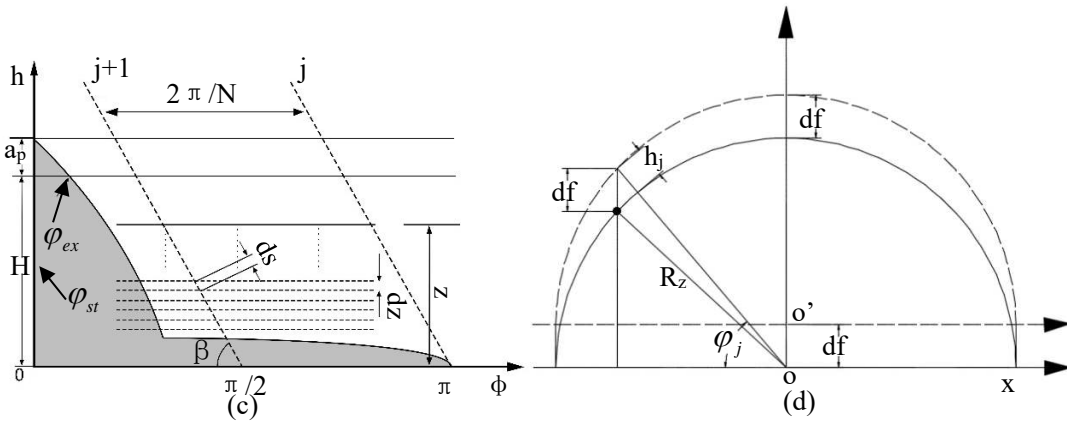

Fig. 2 Illustration of the orbital drilling with ODR tool: (a) tool coordinate and workpiece coordinate, (b) undeformed chip geometry in orbital drilling with ODR tool, (c) illustration of the cutting element, (d) undeformed chip thickness

Then the Eq. 9 can be rewritten as,

$$\begin{cases} dF_{tj} = g\left(\varphi_j\right)\left(K_{tc}h_j\left(\varphi_j,z\right)dz + K_{te}ds\right) \\ dF_{rj} = g\left(\varphi_j\right)\left(K_{rc}h_j\left(\varphi_j,z\right)dz + K_{re}ds\right) \\ dF_{aj} = g\left(\varphi_j\right)\left(K_{ac}h_j\left(\varphi_j,z\right)dz + K_{ae}ds\right) \end{cases} \tag{12}$$

Transform the element coordinate which distributes on the surface of the reaming part to the cutter coordinate $O_tX_tY_tZ_t$, then the cutting force of a cutting edge element can be received as,

$$\begin{cases} dF_{xj}^{tR} = -\cos\left(\varphi_j\right)\cdot dF_{tj} - \sin\left(\varphi_j\right)\cdot dF_{rj} \\ dF_{yj}^{tR} = \sin\left(\varphi_j\right)\cdot dF_{tj} - \cos\left(\varphi_j\right)\cdot dF_{rj} \\ dF_{zj}^{tR} = dF_{aj} \end{cases} \tag{13}$$

The cutting force of reaming part in tool coordinate could be calculated by integrating the element cutting force on the all cutting edges along the tool axis.

$$\begin{cases} F_{xj}^{tR} = \sum_{j=1}^{N}\int_0^H \left(-\cos\left(\varphi_j\right)\cdot dF_{tj} - \sin\left(\varphi_j\right)\cdot dF_{rj}\right)dz \\ F_{yj}^{tR} = \sum_{j=1}^{N}\int_0^H \left(\sin\left(\varphi_j\right)\cdot dF_{tj} - \cos\left(\varphi_j\right)\cdot dF_{rj}\right)dz \\ F_{zj}^{tR} = \sum_{j=1}^{N}\int_0^H dF_{aj}dz \end{cases} \tag{14}$$

Modeling the cutting force of the peripheral cutting edges with the same method, and the cutting force of the ODR tool is expressed as follows,

$$\begin{cases} F_x^t = F_{xj}^{tR} + F_{xj}^{tP} \\ F_y^t = F_{yj}^{tR} + F_{yj}^{tP} \\ F_z^t = F_{zj}^{tR} + F_{zj}^{tP} + F_M \end{cases} \tag{15}$$

The cutting force acting on the workpiece can be obtained by transforming the cutting force in the cutter coordinate to the workpiece coordinate.

$$\begin{cases} F_x^w = F_x^t \cdot \cos\theta_t + F_y^t \cdot \sin\theta_t \\ F_y^w = -F_y^t \cdot \sin\theta_t + F_y^t \cdot \cos\theta_t \\ F_z^w = F_z^t \end{cases} \tag{16}$$

2.2.2 Modeling of temperature distribution of the workpiece

Heat generation and heat transformed into the workpiece

The heat generated in cutting mainly comes from three areas, the primary heat source, owing to the shearing at shear plane; the secondary heat source, because of the friction at the tool-chip interface; the third heat source, due to the friction on the flank surface. In this paper the temperature variation close to the machining area of the workpiece in CFRP orbital drilling is focused, moreover the powder chip has less friction with the rake face. Therefore, the effect of the tool-chip interface friction on workpiece was not taken account. Only the influence of cutting heat from the primary and the secondary heat sources on the workpiece is considered in this paper.

The heat generated during machining is mainly caused by the heat converted from cutting energy. The energy consumption of a cutting element in the first deformation zone can be calculated as Eq. (17). The shear velocity can be deduced from the relationship among the cutting speed and tool angles.

$$\dot{Q}_{fs}(\varphi) = F_s(\varphi) v_s \tag{17}$$

$$v_s = \frac{V \cos\gamma_n}{\cos(\phi_n - \gamma_n)} \tag{18}$$

The heat generated on the shear plane is divided into two parts, one is transferred to the chips and taken away by the chips, the other is transferred to the workpiece, resulting in the temperature rise of the workpiece. The part transferred to the workpiece can be calculated with the method in Ref.[60],

$$\dot{Q}_{fsw} = C_1 \dot{Q}_{fs} \tag{19}$$

Where C_1 is the proportion of the heat transferred to the workpiece to the ones generated in the first deformation zone. According to the Shaw's [61] research, the proportion can be calculated as,

$$C_1 = 1 - \frac{1}{1 + 1.328\sqrt{K_w \varepsilon / v_s h_j(\varphi)}} \tag{20}$$

Where the K_w is the thermal diffusivity of the workpiece, ε is the strain of the chip and can be expressed as $\varepsilon = \cot\phi_n + \tan(\phi_n - \gamma_n)$.

The heat flux of a cutting element in the third deformation zone can be expressed as,

$$\dot{Q}_{tf}(\varphi) = F_f(\varphi) V \tag{21}$$

The heat generated by the friction on the flank face is similar to that by the shear plane. It is also divided into two parts, one is transferred to the tool and the other is transferred to the workpiece, resulting in the temperature rise of the workpiece. The part transferred to the workpiece can be expressed as,

$$\dot{Q}_{tfw} = C_2 \dot{Q}_{tf} \tag{22}$$

Where the C_2 is the ratio of the heat transfer to the workpiece to the heat generated in the third deformation zone. According to the Ref.[32], the proportion can be calculated as,

$$C_2 = 1 - \left(1 + \frac{\pi K_w}{2 h_j(\varphi) V \ln \frac{2b}{l_{wf}}}\right)^{-1} \tag{23}$$

Then the heat flux transfers to the workpiece that generated by a cutting element within one revolution can be expressed as follows,

$$q_{re} = \int_0^{2\pi} \left(g(\varphi_j) \left(C_1 F_s(\varphi) v_s + C_2 F_f(\varphi) V \right) \right) d\varphi \tag{24}$$

Analysis of heat transfer in the workpiece

In the process of orbital drilling, the tool moves along a helical path in a three-

dimensional space, which improves the heat convection of the material at the hole wall and reduces the processing temperature effectively. The heat transfer in CFRP is relatively complex for the different thermal conductivities in different directions, the short processing time and the heat accumulates in the workpiece induce an unsteady state which makes it more difficult to predict the temperature of orbital drilling in CFRP. Therefore, most models of temperature field for milling or grinding are not suitable for predicting the temperature field of orbital drilling on CFRP. A three-dimensional, unsteady state heat transfer equation considering convective heat transfer was established in this paper. For getting the variation of the magnitude and distribution of workpiece temperatures, the finite difference method was used to solve the heat conduction equation. When solving the equation with finite different, it is necessary to approximate the shape of the hole wall with nodes. However, different calculation methods of convective heat transfer for nodes, internal and external angular points may affect the accuracy of the calculation in rectangular coordinates. The application of Cartesian coordinates in the calculation is conducive to the accuracy of mathematics and the realization of model calculation. And it is more consistent with the physical process of heat diffusion. Therefore, the heat transfer equation in polar coordinates which is used to calculate the temperature field distribution of orbital drilling on CFRP is presented in equations (25)-(27).

$$\lambda_1 \frac{\partial^2 T}{\partial r^2} + \lambda_1 \frac{1}{r_w} \frac{\partial T}{\partial r} + \lambda_2 \frac{1}{r_w{}^2} \frac{\partial^2 T}{\partial \theta^2} + \lambda_3 \frac{\partial^2 T}{\partial z^2} + q(r_w, \theta_w, \mathrm{z}_w, \mathrm{t}) = \rho c \frac{\partial T}{\partial t} \tag{25}$$

Initial conditions,

$$T = T_0 \tag{26}$$

Boundary conditions,

$$-\lambda_1 \frac{\partial T}{\partial n} = h\left(T - T_0\right) \tag{27}$$

Where the $q(r_w, \theta_w, \mathrm{z}_w, \mathrm{t})$ is the heat flux generated of the heat source. Heat conductivities in x , y , z directions of unidirectional prepreg are different. Multidirectional CFRP was studied in this paper to simplify the calculation process, assuming the heat conductivities of the workpiece in the y is the same as that in the x direction. From Eqs. (25)-(27), the heat transfer problem can be treated as a workpiece with different heat conductivity in the horizontal and vertical directions being placed in an environment with temperature T_0 . The approximations which have been made as Eq. (28) and (29), for rewriting the partial differential equation to a finite difference form. And the position of each node in the meshing of the workpiece is shown in Fig.3.

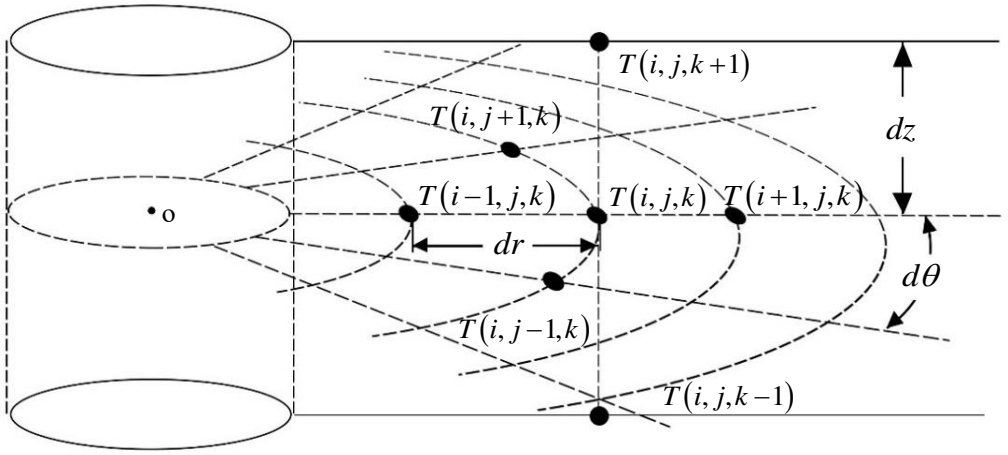

Fig. 3 Diagram of the workpiece meshing

$$\frac{\partial T}{\partial t}=\frac{T\left(i,j,k,t+1\right)-T\left(i,j,k,t\right)}{\Delta t} \tag{28}$$

$$\begin{aligned}
&\frac{1}{r_w}\frac{\partial T}{\partial r}=\frac{1}{2r_w\Delta r}\left(T\left(i+1,j,k\right)-T\left(i-1,j,k\right)\right)\\
&\frac{\partial^2 T}{\partial r^2}=\frac{1}{\Delta r^2}\left(T\left(i+1,j,k\right)+T\left(i-1,\mathrm{j},\mathrm{k}\right)-2T\left(i,j,k\right)\right)\\
&\frac{1}{r_w^{\,2}}\frac{\partial^2 T}{\partial \theta^2}=\frac{1}{r_w^{\,2}\Delta\theta^2}\left(T\left(i,j+1,k\right)+T\left(i,j-1,k\right)-2T\left(i,j,k\right)\right)\\
&\frac{\partial^2 T}{\partial z^2}=\frac{1}{\Delta z^2}\left(T\left(i,j,k-1\right)+T\left(i,j,k+1\right)-2T\left(i,j,k\right)\right)
\end{aligned} \tag{29}$$

Therefore, with the help of the above approximations, the partial differential heat transfer equation in polar coordinates (Eq.(25)) has been reorganized as the following finite difference forms,

$$\begin{aligned}
&T\left(i,j,k,t+1\right)=\\
&T\left(i,j,k,t\right)+\Delta t\left(\begin{array}{l}
\dfrac{\lambda_1}{\rho c}\left(\begin{array}{l}\dfrac{1}{2r_w\Delta r}\left(T\left(i+1,j,k,t\right)-T\left(i-1,j,k,t\right)\right)\\ +\dfrac{1}{\Delta r^2}\left(T\left(i+1,j,k,t\right)+T\left(i-1,\mathrm{j},\mathrm{k},t\right)-2*T\left(i,j,k,t\right)\right)\end{array}\right)\\
+\dfrac{\lambda_2}{\rho c}\left(\dfrac{1}{r_w^{\,2}\Delta\theta^2}\left(T\left(i,j+1,k,t\right)+T\left(i,j-1,k,t\right)-2*T\left(i,j,k,t\right)\right)\right)\\
+\dfrac{\lambda_3}{\rho c}\left(\dfrac{1}{\Delta z^2}\left(T\left(i,j,k+1,t\right)+T\left(i,j,k-1,t\right)-2*T\left(i,j,k,t\right)\right)\right)\\
+\dfrac{q\left(r_w,\theta_w,z_w,t\right)}{\rho c}
\end{array}\right)
\end{aligned} \tag{30}$$

Moving heat source in the workpiece

It can be seen from the analysis of the cutting force of a cutting element above, the force generated by the element is a function of undeformed chip thickness and cutting force coefficient. The coefficient is determined by the geometric of the tool, thus the cutting force generated by the element is only affected by the undeformed chip thickness. The direction and the magnitude variations of cutting force of the tool are caused by the rotation angle and the number of the elements involving in cutting.

It can be observed from Eq.(17) and Eq.(21), the energy consumption of a cutting element in cutting process can be calculated by cutting force and cutting speed. The heat flux produced by the element in steady cutting is a periodic function of the rotation angle. Therefore, the heat transfer process of milling and grinding can be regarded as the heat transfer process caused by the movement of a heat source with the fixed shape along the tool path.

In previous studies, the heat source is mostly simplified as a moving curve or a moving surface with a regular shape. However, in orbital drilling, the cutting heat is generated by both the bottom edge and peripheral cutting edge, and the heat transfer process is more complex when the tool moves along the helical path. It is difficult to simulate the heat conduction process of the orbital drilling with a simple moving heat source, and it is also too difficult to get the solution.

The contact area between the ODR tool and the workpiece during steady cutting is shown in Fig. 2b and c. It can be observed from Eq. 10 that the influence of cutting edge rotation angle on chip thickness is more significant than that of tool radius. According to Eq.24, it can be seen that the heat flux generated by the cutting element during the processing is related to the rotation angle (φ)and the height (z) of the cutting element, but not to the position of the tool. That is, the shape and heat distribution of the heat source formed on the cutting tool remains constant. Therefore, the heat transfer problem of orbital drilling can be treated as a complex curved surface heat source moving along a helical path in the workpiece, which has the same shape of the contact area between the tool and the workpiece. The heat transfer occurs between the nodes inside the workpiece and the moving heat source. The material which the heat source passed through is removed, assuming the temperature of the nodes that the heat source passed through changes into the ambient temperature, and convects heat with the newly formed boundary.

3 Experimental work

3.1Properties of cutting tools and workpiece

For verifying the usability of the cutting force model and the heat transfer model, a

series of cutting tests were carried out with dedicated tools and general end mills. The parameters of the tools in the experiments are listed in Table 1.

Table 1 Details of the cutters

Tool type	Feature	Value
General end mill	Tool diameter	8 mm
	Carbide	K20
	Helix angle	30°
	Coated	No
	Flutes	4
	Rake angle of the end teeth and peripheral cutting edges	7°
	Tool clearance of the end teeth and peripheral cutting edges	7°
ODR tool	Diameter of the milling part	5.5 mm
	Diameter of the peripheral cutting edges	8 mm
	Radius of the arc of the ODR tool	10.625mm
	Height of the reaming part	5 mm
	Carbide	K20
	Helix angle	30°
	Coated	No
	Flutes	4
	Rake angle of the milling part, reaming part and peripheral cutting edges	7°
	Tool clearance of the milling part, reaming part and peripheral cutting edges	7°

The workpiece was a multi-direction CFRP plate, which made from 3k plain unidirectional prepreg with epoxy resin as the matrix material. After compression molding and high temperatures curing, the workpiece which had two plies of woven prepreg as top and bottom, and 36 unidirectional plies with symmetrical layout [0°,+45°,90°,-45°]9s as middleware, was cut into 90mm×90mm×5 mm. The tensile strength of the composite was 2400 MPa, and the Young's modulus was 160 GPa.

Table 2 Thermal properties of the CFRP workpiece

Heat conductivity of workpiece in x direction	$\lambda_1 = 4.18$	$W \cdot (m \cdot K)^{-1}$
Heat conductivity of workpiece in y direction	$\lambda_2 = 4.18$	$W \cdot (m \cdot K)^{-1}$
Heat conductivity of workpiece in z direction	$\lambda_3 = 0.76$	$W \cdot (m \cdot K)^{-1}$
Heat capacity of the workpiece	c=990	$J \cdot (kg \cdot K)^{-1}$
Density of the workpiece	ρ=1520	$kg \cdot m^{-3}$
Convective heat transfer coefficient	$h = 75$	$W \cdot (m^2 \cdot K)^{-1}$

3.2Design of experiments

The cutting force coefficients were demarcated according to the methods in Ref.[62]. The modeling process of cutting force in orbital drilling is similar to that of milling, and the difference of cutting force model in orbital drilling is that the cutting edge involved in processing is more complex, and the cutting force needs to be transformed into workpiece coordinate in the end. According to Ref.[63], the cutting force coefficients of different parts in the tool were acquired respectively. Obviously, the transformation of the coordinate does not change the magnitude of force. Thus, the cutting force coefficients of the reaming part and the periphery cutting edge can be obtained in flank milling tests, and the coefficients of milling part in ODR tool and end mill can be obtained in plunge milling tests. The experiments were carried out on VM7032 CNC milling machine, Kistler 9257B dynamometer and Kistler 5070 amplifier were used to measure and record the cutting force. The experimental setup is shown in Fig. 4. The flank milling tests for reaming part and periphery cutting edge were carried out with a tool rotational speed of 1000rpm, a cutting depth of 5mm and four levels of the feed rate (f=0.01, 0.02, 0.04, 0.08 mm/rev), and the plunge milling tests were executed with the same rotational speed and feed rate, and cylindrical workpiece with different diameters (2mm, 3mm, 4mm, 5mm, 6mm, 7mm, 8mm). In order to verify the validity of the cutting force model for the end mill and the ODR tool, the same experimental setup was used in the experiments. And the tests were executed with an eccentricity of 1mm, a tangential feed rate of v_{ft}=0.126 mm/rev, a Z-axis feed rate of v_{fa}=0.02 mm/rev, and a tool rotational speed of 1000 rpm.

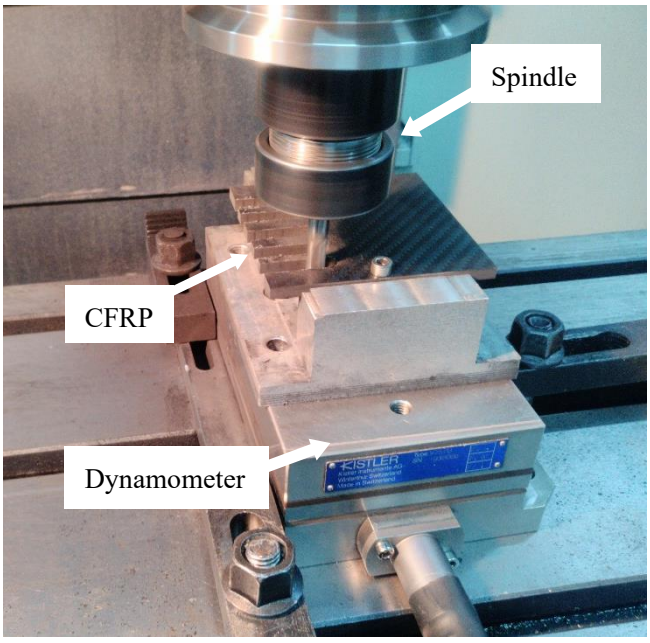

Fig.4 The experimental setup in cutting force coefficient identification experiment

To verify the validity of the temperature distribute model, a verification experiment was carried out. For measuring the cutting temperature at the hole wall during machining, FLIR A320 Tempscreen thermal infrared imager and a close-up lens 4X were used in the test. In order to facilitate the thermal imager shooting and to avoid the influence of uneven thickness of material, semicircles with radius of 6mm, 7mm, 8mm, 9mm around

the hole for predicting different material thicknesses were made on the workpiece to verify the accuracy of the model. Three points were marked in the infrared image to show the temperatures of three points at different heights of the sidewall. Sp2 is 2.5mm away from the top layer of the workpiece, Sp1 is the midpoint between the top layer of the workpiece and Sp2, Sp3 is the midpoint between the bottom of the workpiece and Sp2. The experimental setups are illustrated in Fig.5. The cutting conditions were listed in Table 3. In order to avoid chips blocking the shooting, the flowing air was used to remove the chips, and all the experiments adopted dry machining.

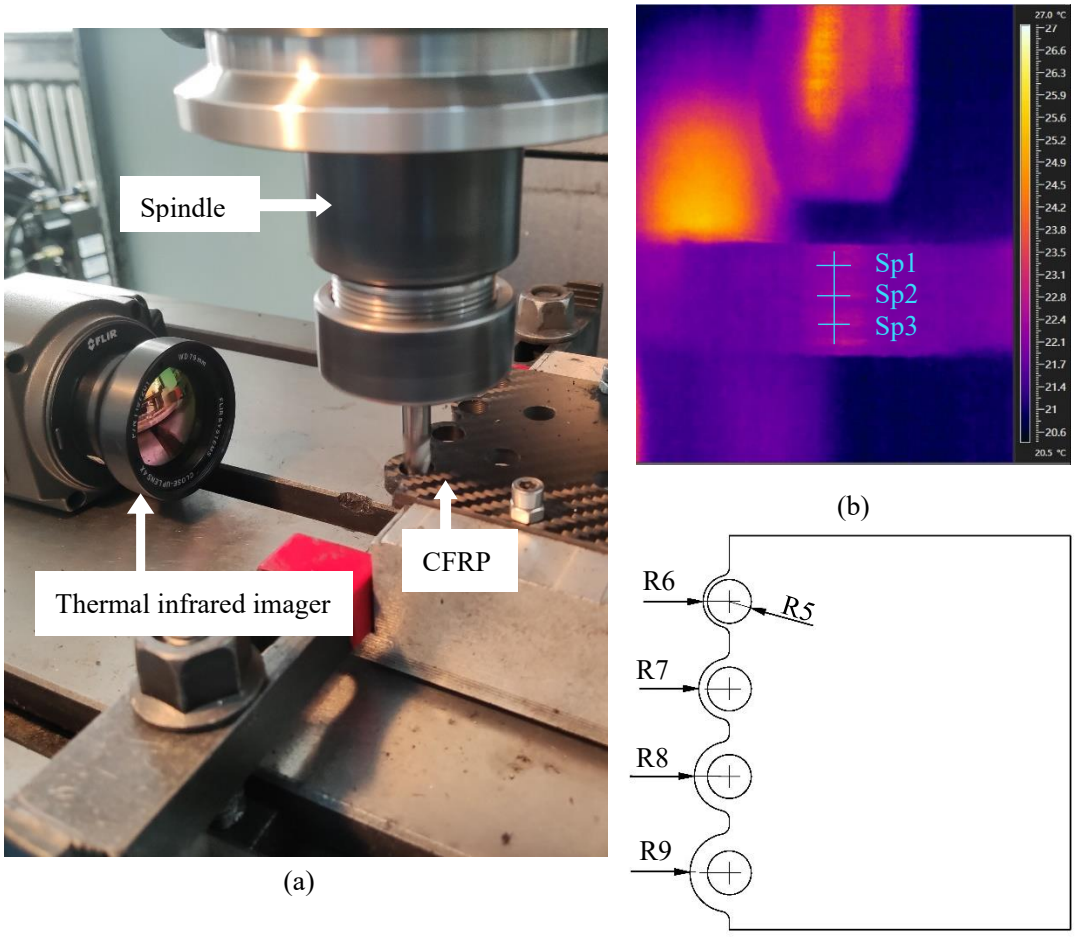

(a) (b) (c)

Fig. 5 (a) Experimental setup in test 2 and (b) infrared image of the workpiece (c) the workpiece in verification experiment of temperature distribute model

Table 3 Cutting parameters in verification experiment of the temperature distribute model

	a_p (mm)	e (mm)	ft (mm/r)	fz (mm/r)	n_t (r/min)
Ⅰ	1	1	0.063	0.01	1000
Ⅱ	0.5	1	0.063	0.005	1500

4 Results and discussion

4.1 Verification of the cutting force model

With consideration of the tool shape, tool path and cutting process, a cutting force model for orbital drilling is established in this paper. However, the shape and parameters of the tool, the material of the workpiece and the cutting parameters all have impacts on the cutting force. To predict the cutting force of orbital drilling with ODR tool, the cutting force coefficient identification experiment was carried out. The coefficient of the cutting edges in the reaming part and the peripheral cutting edges were identified with the method in Ref.[64], and the coefficients of the cutting edges in the milling part were identified with the method in Ref. [63] and [65]. The average cutting force in steady cutting is used to identify the cutting force coefficient, and the coefficient of ODR tool are listed in Table 4. The end mill employed in this research has the same parameters with the ODR tool, assuming that the end mill has the same cutting force coefficient with the peripheral cutting edges and the edges on the milling part of the ODR tool.

Table 4 Cutting force coefficient

The reaming part	K_{tc}	K_{te}	K_{rc}	K_{re}	K_{ac}	K_{ae}
	636.00	3.74	735.90	11.65	-134.99	0.76
Peripheral cutting edges	K_{ptc}	K_{pte}	K_{prc}	K_{pre}	K_{pac}	K_{pae}
	580.50	5.02	866.40	13.32	-220.38	-0.99
Milling part		K_{mac}			K_{mae}	
		269.90* D_t			16.93* D_t	

As can be observed in Table 4, the cutting force coefficient K_{pac}, K_{pae} are negative, which means that the thrust force generated by the cutting edges on the peripheral cutting edges of an end mill and an ODR tool is upward. The cutting force coefficient K_{ac} is negative, and K_{ae} is positive, which means that the direction of the thrust force generated by the cutting edges of the reaming part is affected by the cutting parameters. The thrust force generated by the reaming part is positive when the tangential feed per tooth is small. The thrust force gradually decreases to a negative value with the increase of tangential feed rate, and the direction changes. Therefore the thrust force in orbital drilling is almost all produced by the edges at the bottom of the end mill and the ODR tool. And the magnitude of the thrust force is positively correlated with the diameter of the cutting edges at the bottom. The prediction of cutting force model and the experimental result of ODR are shown in Fig. 6.

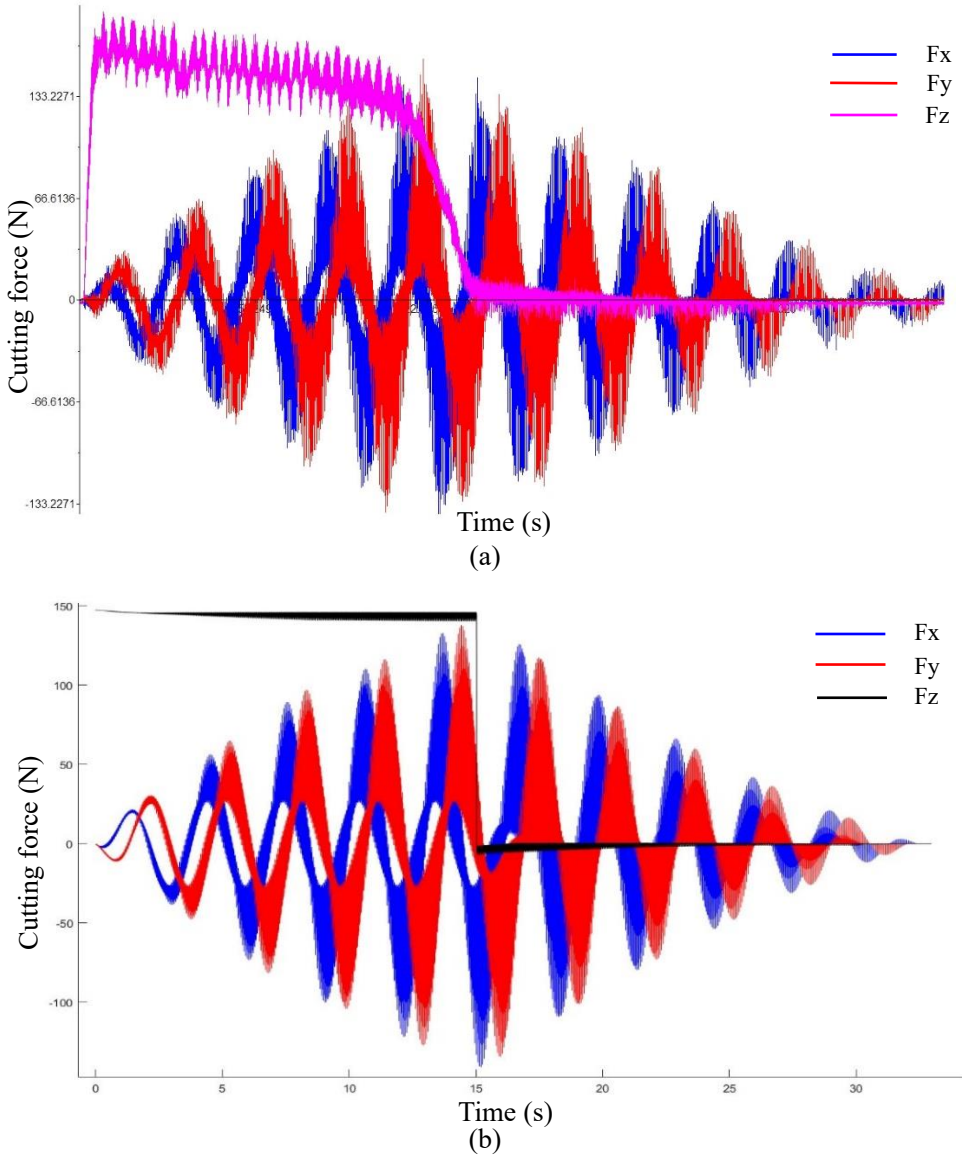

Fig.6 Prediction and experimental result: (a) experimental result, (b) prediction of cutting force model

As can be observed in Fig.6a, at the beginning of the machining the thrust force soars to the maximum value, the cutting force in x, y directions are affected by the planetary motion of the tool, which changes periodically. The cutting force increases gradually while the reaming part penetrates into the workpiece, and the cutting force in x, y directions reach the maximum when the reaming part enters the workpiece completely. The thrust force decreases rapidly to zero, when the milling part passes through the bottom of the workpiece, and the cutting force in x, y directions begin to decrease gradually. As the presented in Fig. 6b, the prediction of the model is consistent with the experimental result. The cutting force model can well predict the magnitude and trend of cutting force in x, y, z direction. But the model cannot show the thrust force decreases with the increase of the machining depth which probably caused by the workpiece deformation. The same prediction result was obtained in the orbital drilling with the end mill. Thus the model could be used to predict the cutting force of the end mill and the ODR tool in orbital drilling.

4.2 Verification of the temperature distribution model

In the verification of the heat transfer model, at first the heat fluxes generated by two kinds of cutting tools were calculated with the experimental condition (an eccentricity of 1mm, a tangential feed rate of v_{ft}=0.063 mm/rev, a Z-axis feed rate of v_{fa}=0.01 mm/rev, and a tool rotational speed of 1000 rpm).

The heat generated by peripheral cutting edges and the edges of the reaming part act on the hole wall directly, and causes the most apparent effect on the temperature rise. Therefore, the heat fluxes produced by peripheral cutting edge and the edge on the reaming part of two kinds of tools were shown in Fig. 7. Taking the hole wall formed at the top of the workpiece when the cutter first contacting the workpiece as an example, the heat fluxes generated by a cutting edge of the end mill in a cycle is marked by a red line. According to the cutting parameters, the materials on the hole wall will be cut six times by the ODR tool, the heat fluxes and the action times are labelled by bule.

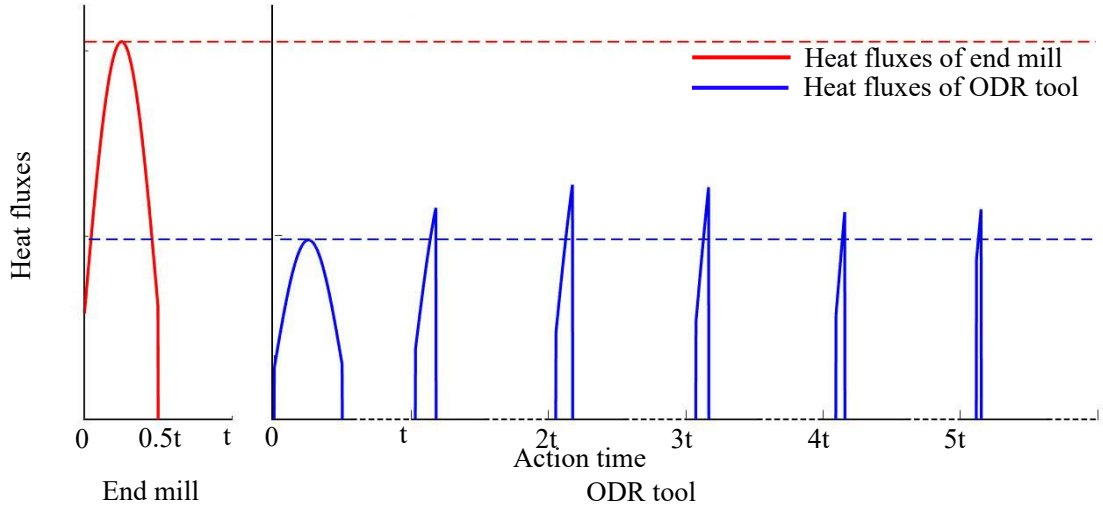

Fig.7 Heat fluxes of the peripheral cutting edge and the edge on the reaming part of two kinds of tools

It can be observed from Fig. 7, the cutting edge of an end mill generates the heat between 0° and 180° in a rotational period, and the heat flux changes as sine functions due to the influence of chip thickness. In the first cutting revolution, the heat flux generated by the cutting edge of ODR has the same trend as that of the end mill, and the heat fluxes are less than that of the end mill due to a low cutting speed. The maximum value of heat flux increases in the 2^{nd} to 6^{th} machining cycle due to the increase of tool radius and the change of chip thickness. However, affected by the undeformed chip geometry, the action time decreases gradually. The total heat flux generated by the ODR cutter is less than that of the end mill, and ODR tool disperses the heat in multiple processing revolutions and gradually acts on the workpiece, makes full use of the heat dissipation process in each processing revolutions to reduce the temperature of workpiece.

In this paper, the calculated results of the heat transfer model are compared with the

experimental results which measured by the infrared thermal imager. The results are shown in Fig. 8.

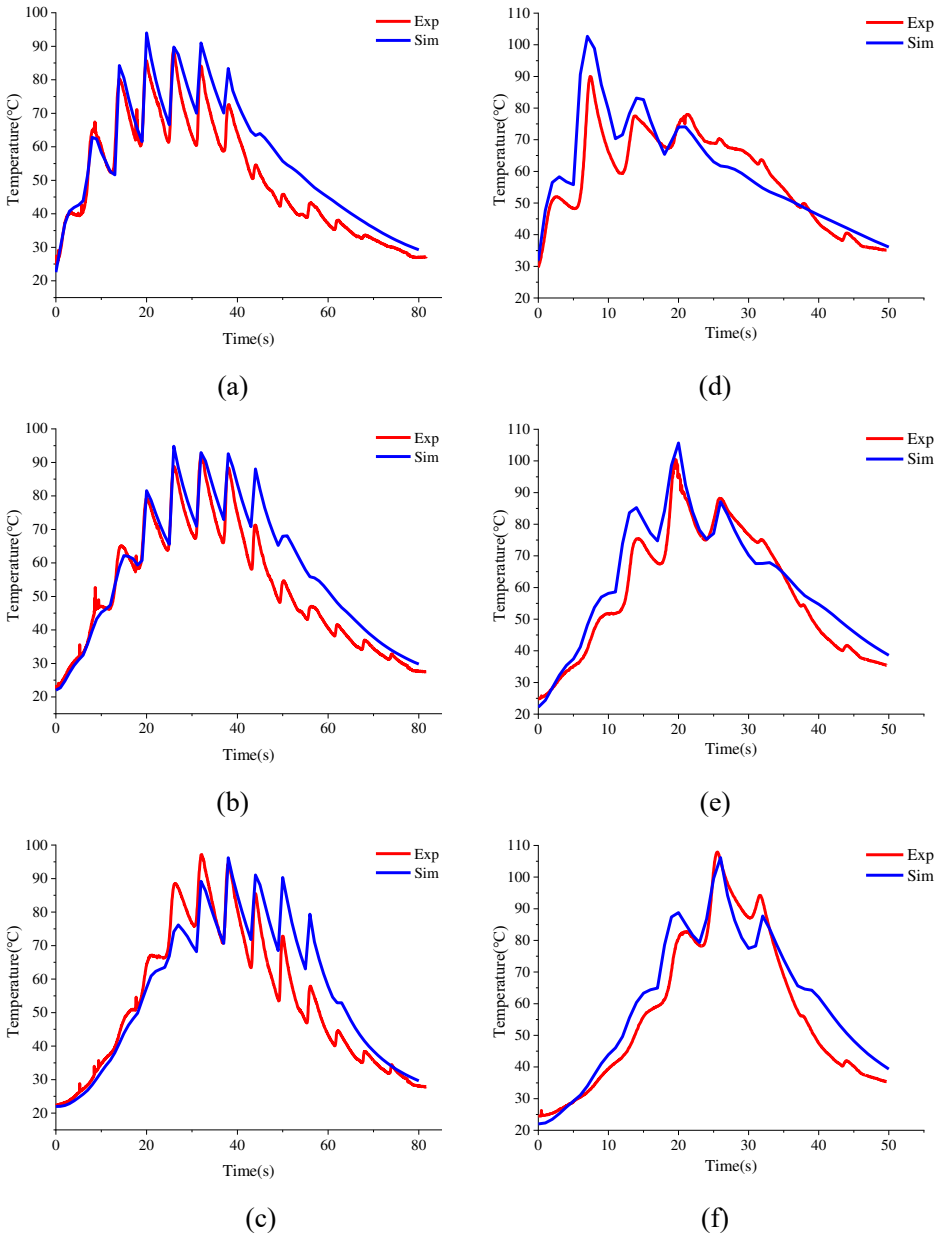

Fig.8 Comparison of simulation results and experimental results of machining temperature: (a) results comparison of ODR at sp1, (b) results comparison of ODR at sp2, (c) results comparison of ODR at sp3, (d) results comparison of end mill at sp1,(e) results comparison of end mill at sp2,(f) results comparison of end mill at sp3,

The graphs in Fig.8 show the comparison of simulation and experimental results of machining temperature at different marked points of the ODR tool and the end mill. As presented in Fig.8, ODR tool has a lower cutting temperature at every marked point. Owing to the multiple expansion by reaming part, the processing revolutions of the ODR tool at each point are much more than that of the end mill, and the temperature rise produced by each processing of ODR is significantly lower than that of the end mill. The workpiece temperature accumulation of the end mill is much more obvious

than that of the ODR tool. As can be observed from Fig. 8c and 8f, the highest cutting temperature both appears at the marked points near the bottom for two kinds of tools. The comparison of the simulation and experimental results shows that the temperature distribution model can predict the change of workpiece temperature field during machining. While, as the presentations of Fig.8 a, b, c and d, e, f, there is no obvious distinction among the maximum temperatures of the three marked points, it is probably because the temperature distribution model, which takes the heat flux generated by the tool during steady cutting as the moving heat source, ignores the temperature change of the tool in the machining process. The temperature distribution model does not take the heat into account which generated by the friction between the cutting edge and the machined surface after machining, therefore the serrated temperature fluctuations in the last stage are not presented in graphs in Fig.8. The simulation results and the experimental results show that the processing temperature of the marked point near the bottom of the workpiece is the highest, and the high processing temperature is easy to cause defect, which is also consistent with the defect always existing at hole exit. Fig.9 shows the experimental and simulation results of sp3's temperature in two groups of tests for ODR tool and end mill at different material thicknesses of sp3.

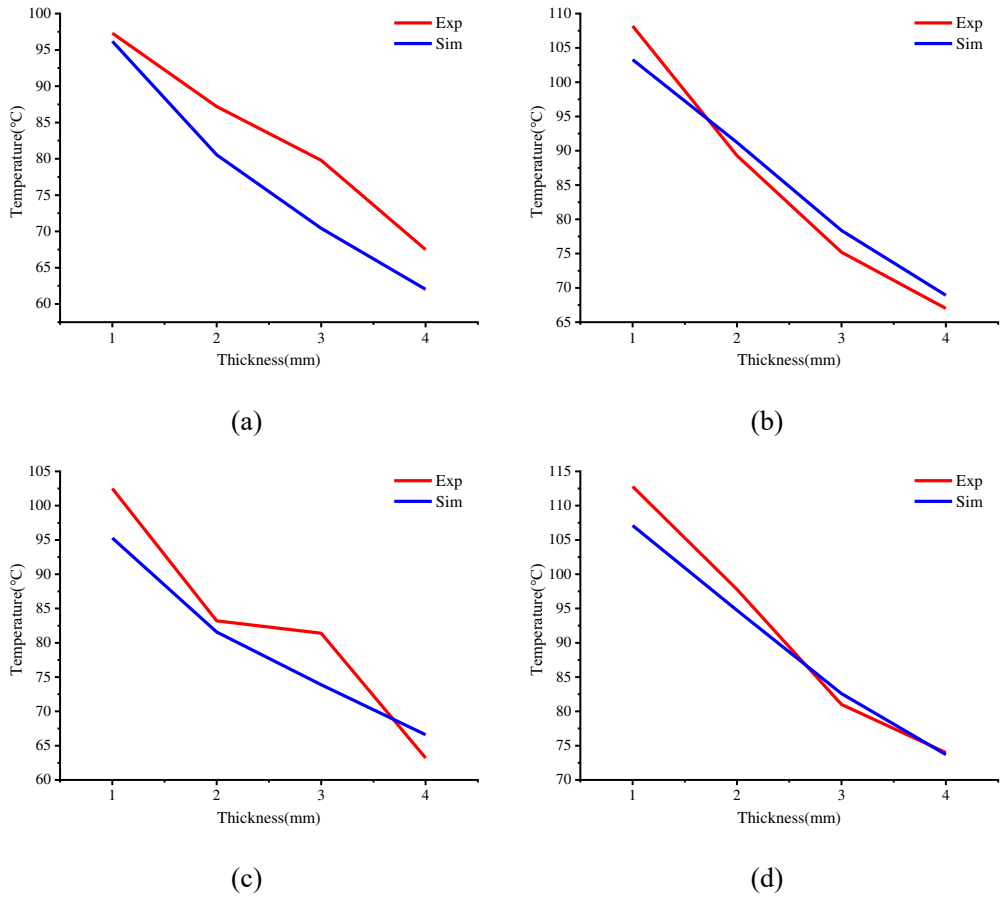

Fig.9 Maximum processing temperature of experimental results and simulation results: (a) results of ODR tool in cutting condition I, (b) results of end mill in cutting condition I, (c) results of ODR tool in cutting condition II, (d) results of end mill in cutting condition II

As can be observed from Fig.9, processing with the same cutting parameters, the cutting

temperature of end mill is higher than that of ODR. The temperature of material close to the hole wall is the highest in horizontal direction, and the temperature of the marked point decreases gradually with the increase of the thickness of the material. Therefore, the matrix near to the hole wall is prone to melt mostly. As can be observed from Fig.9 a-d, the experimental results have the same trend with the simulation results. Although the temperature distribution model cannot predict the processing temperature accurately, the errors between the predicted results and the experimental results are mostly less than 15%.

5 Conclusion

In this paper, the cutting temperature of orbital drilling in CFRP of two kinds of tools were studied. A numerical model which was solved by the finite difference method was carried out to predict the unsteady state three-dimensional heat conduction process. The proposed temperature distribute model is capable to reappear the changing of the temperature field inside the workpiece. The following conclusions are gained:

1. For end mill and ODR tools, the thrust force is all generated by the cutting edge at the bottom of the tool, and the thrust force generated by the peripheral cutting edge and the edge on the reaming part is upward in orbital drilling. The magnitude of the thrust force produced by the tool is related to the diameter of the cutting edge at the bottom.
2. The total heat generated by the ODR tool is lower than that generated by the end mill, and the heat is dispersed in multiple processing revolutions and gradually acts on the workpiece. Therefore, the processing temperature of ODR tool is lower than that of the end mill.
3. The finite difference method was used for the solutions of the unsteady-state heat transfer equation. The temperature field predicted by the temperature distribute model has small errors compared with the experimental results. The model can be utilized for predicting the cutting temperature inside the workpiece during orbital drilling of CFRP.
4. During machining, the processing temperature near the exit of the hole wall is higher than that near the entrance. The temperature of the material near the hole wall inside the workpiece is higher and the temperature gradually decreases with the increase of the distance. Therefore, the machining temperature of the material near the exit is the highest, and the matrix is the most vulnerable to soften, which is also one of the reasons why the processing defect mostly occurs at the exit.

Funding information

This work was supported by the National Key Research and Development Program of

China under Grant No. 2019YFB1704803.

References

1. Gao YF, Xiong J, Xiao JH, Lu D (2019) A tilted orbital grinding technique for hole-making of CFRP composite laminates. Int J Adv Manuf Tech 104 (1-4):661-673. doi:10.1007/s00170-019-03904-x

2. Wang CY, Chen YH, An QL, Cai XJ, Ming WW, Chen M (2015) Drilling Temperature and Hole Quality in Drilling of CFRP/Aluminum Stacks Using Diamond Coated Drill. Int J Precis Eng Manuf 16 (8):1689-1697. doi:10.1007/s12541-015-0222-y

3. Ben W, Hang G, Quan W, Maoqing W, Songpeng Z (2012) Influence of Cutting Heat on Quality of Drilling of Carbon/Epoxy Composites. Mater Manuf Process 27 (9):968-972. doi:10.1080/10426914.2011.610079

4. Bonnet C, Poulachon G, Rech J, Girard Y, Costes JP (2015) CFRP drilling: Fundamental study of local feed force and consequences on hole exit damage. Int J Mach Tool Manu 94:57-64. doi:10.1016/j.ijmachtools.2015.04.006

5. Feito N, Diaz-Alvarez J, Lopez-Puente J, Miguelez MH (2018) Experimental and numerical analysis of step drill bit performance when drilling woven CFRPs. Compos Struct 184:1147-1155. doi:10.1016/j.compstruct.2017.10.061

6. Durao LMP, Goncalves DJS, Tavares JMRS, de Albuquerque VHC, Vieira AA, Marques AT (2010) Drilling tool geometry evaluation for reinforced composite laminates. Compos Struct 92 (7):1545-1550. doi:10.1016/j.compstruct.2009.10.035

7. Su F, Zheng L, Sun FJ, Wang ZH, Deng ZH, Qiu XY (2018) Novel drill bit based on the step-control scheme for reducing the CFRP delamination. J Mater Process Tech 262:157-167. doi:10.1016/j.jmatprotec.2018.06.037

8. Isbilir O, Ghassemieh E (2013) Numerical investigation of the effects of drill geometry on drilling induced delamination of carbon fiber reinforced composites. Compos Struct 105:126-133. doi:10.1016/j.compstruct.2013.04.026

9. Qiu XY, Li PN, Niu QL, Chen AH, Ouyang PR, Li CP, Ko TJ (2018) Influence of machining parameters and tool structure on cutting force and hole wall damage in drilling CFRP with stepped drills. Int J Adv Manuf Tech 97 (1-4):857-865. doi:10.1007/s00170-018-1981-2

10. Butler-Smith PW, Axinte DA, Dame M, Kennedy AR, Harper LT, Bucourt JF, Ragueneau R (2015) A study of an improved cutting mechanism of composite materials using novel design of diamond micro-core drills. Int J Mach Tool Manu 88:175-183.

doi:10.1016/j.ijmachtools.2014.10.002

11. Hocheng H, Tsao CC (2005) The path towards delamination-free drilling of composite materials. J Mater Process Tech 167 (2-3):251-264. doi:10.1016/j.jmatprotec.2005.06.039

12. Qiu XY, Li PN, Li CP, Niu QL, Chen AH, Ouyang PR, Ko TJ (2018) Study on chisel edge drilling behavior and step drill structure on delamination in drilling CFRP. Compos Struct 203:404-413. doi:10.1016/j.compstruct.2018.07.007

13. Tsao CC (2008) Experimental study of drilling composite materials with step-core drill. Mater Design 29 (9):1740-1744. doi:10.1016/j.matdes.2008.03.022

14. Zimmermann M, Heberger L, Schneider F, Effgen C, Aurich JC (2016) Investigation of chip formation and workpiece load when machining carbon-fiber-reinforced-polymer (CFRP). 16th Machining Innovations Conference for Aerospace Industry - Mic 2016 6:124-131. doi:10.1016/j.promfg.2016.11.016

15. Shyha IS, Aspinwall DK, Soo SL, Bradley S (2009) Drill geometry and operating effects when cutting small diameter holes in CFRP. Int J Mach Tool Manu 49 (12-13):1008-1014. doi:10.1016/j.ijmachtools.2009.05.009

16. Iliescu D, Gehin D, Gutierrez ME, Girot F (2010) Modeling and tool wear in drilling of CFRP. Int J Mach Tool Manu 50 (2):204-213. doi:10.1016/j.ijmachtools.2009.10.004

17. Pereira RBD, Brandao LC, de Paiva AP, Ferreira JR, Davim JP (2017) A review of helical milling process. Int J Mach Tool Manu 120:27-48. doi:10.1016/j.ijmachtools.2017.05.002

18. Brinksmeier E, Fangmann S, Meyer I (2008) Orbital drilling kinematics. Prod Eng 2 (3):277-283. doi:10.1007/s11740-008-0111-7

19. Geier N, Davim JP, Szalay T (2019) Advanced cutting tools and technologies for drilling carbon fibre reinforced polymer (CFRP) composites: A review. Compos Part a-Appl S 125. doi:10.1016/j.compositesa.2019.105552

20. Pereszlai C, Geier N (2020) Comparative analysis of wobble milling, helical milling and conventional drilling of CFRPs. Int J Adv Manuf Tech 106 (9-10):3913-3930. doi:10.1007/s00170-019-04842-4

21. Xu WX, Zhang LC (2014) On the mechanics and material removal mechanisms of vibration-assisted cutting of unidirectional fibre-reinforced polymer composites. Int J Mach Tool Manu 80-81:1-10. doi:10.1016/j.ijmachtools.2014.02.004

22. Alberdi A, Suarez A, Artaza T, Escobar-Palafox GA, Ridgway K (2013) Composite Cutting with Abrasive Water Jet. Manufacturing Engineering Society International Conference, (Mesic 2013) 63:421-429. doi:10.1016/j.proeng.2013.08.217

23. Herzog D, Jaeschke P, Meier O, Haferkamp H (2008) Investigations on the thermal effect caused by laser cutting with respect to static strength of CFRP. Int J Mach Tool Manu 48 (12-13):1464-1473. doi:10.1016/j.ijmachtools.2008.04.007

24. Teicher U, Muller S, Munzner J, Nestler A (2013) Micro-EDM of carbon fibre-reinforced plastics. Proc 17th Cirp Conf Ele Phy Chem Mach (Isem) 6:320-325. doi:10.1016/j.procir.2013.03.092

25. Wang Q, Wu Y, Bitou T, Nomura M, Fujii T (2017) Proposal of a tilted helical milling technique for high quality hole drilling of CFRP: kinetic analysis of hole formation and material removal. Int J Adv Manuf Tech 94 (9-12):4221-4235. doi:10.1007/s00170-017-1106-3

26. Voss R, Henerichs M, Kuster F (2016) Comparison of conventional drilling and orbital drilling in machining carbon fibre reinforced plastics (CFRP). Cirp Annals-Manuf Tech 65 (1):137-140. doi:10.1016/j.cirp.2016.04.001

27. Wang GD, Kirwa MS, Li N (2018) Experimental studies on a two-step technique to reduce delamination damage during milling of large diameter holes in CFRP/Al stack. Compos Struct 188:330-339. doi:10.1016/j.compstruct.2018.01.039

28. Taylor, Fred W (1907) The Art of Cutting Metals. Scientific American 63 (1618supp):25929-25931

29. Komanduri R, Hou ZB (2000) Thermal modeling of the metal cutting process - Part I - Temperature rise distribution due to shear plane heat source. Int J Mech Sci 42 (9):1715-1752. doi:Doi 10.1016/S0020-7403(99)00070-3

30. Komanduri R, Hou ZB (2001) Thermal modeling of the metal cutting process — Part II: temperature rise distribution due to frictional heat source at the tool–chip interface. Int J Mech Sci 43 (1):57-88. doi:10.1016/s0020-7403(99)00104-6

31. Komanduri R, Hou ZB (2001) Thermal modeling of the metal cutting process — Part III: temperature rise distribution due to the combined effects of shear plane heat source and the tool–chip interface frictional heat source. Int J Mech Sci 43 (1):89-107. doi:10.1016/s0020-7403(99)00105-8

32. Berliner EM, Krainov VP (1991) Analytic Calculations of the Temperature-Field and Heat Flows on the Tool Surface in Metal-Cutting Due To Sliding Friction. Wear 143 (2):379-395. doi:Doi 10.1016/0043-1648(91)90108-7

33. Lin S, Peng FY, Wen J, Liu YZ, Yan R (2013) An investigation of workpiece temperature variation in end milling considering flank rubbing effect. Int J Mach Tool Manu 73:71-86. doi:10.1016/j.ijmachtools.2013.05.010

34. Zhang J, Liu Z, Du J (2016) Prediction of cutting temperature distributions on rake face of coated cutting tools. Int J Adv Manuf Tech 91 (1-4):49-57. doi:10.1007/s00170-016-9719-5

35. Richardson DJ, Keavey MA, Dailami F (2006) Modelling of cutting induced workpiece temperatures for dry milling. Int J Mach Tool Manu 46 (10):1139-1145. doi:10.1016/j.ijmachtools.2005.08.008

36. Huang Y, Liang SY (2005) Cutting temperature modeling based on non-uniform

heat intensity and partition ratio. Mach Sci Tech 9 (3):301-323. doi:10.1080/10910340500196421

37. Bäker M (2006) Finite element simulation of high-speed cutting forces. J Mater Process Tech 176 (1-3):117-126. doi:10.1016/j.jmatprotec.2006.02.019

38. Li R, Shih AJ (2005) Finite element modeling of 3D turning of titanium. Int J Adv Manu Tech 29 (3-4):253-261. doi:10.1007/s00170-005-2511-6

39. Umbrello D, M'Saoubi R, Outeiro JC (2007) The influence of Johnson–Cook material constants on finite element simulation of machining of AISI 316L steel. Int J Mach Tool Manu 47 (3-4):462-470. doi:10.1016/j.ijmachtools.2006.06.006

40. Dutt RP, Brewer RC (1965) On the Theoretical Determination of the Temperature Field in Orthogonal Machining. Int J prod Res 4 (2):91-114. doi:10.1080/00207546508919968

41. Lazoglu I, Altintas Y (2002) Prediction of tool and chip temperature in continuous and interrupted machining. Int J Mach Tool Manu 42 (9):1011-1022. doi:10.1016/S0890-6955(02)00039-1

42. Liu J, Ren CZ, Qin XD, Li H (2014) Prediction of heat transfer process in helical milling. Int J Adv Manuf Tech 72 (5-8):693-705. doi:10.1007/s00170-014-5662-5

43. Liu J, Chen G, Ji CH, Qin XD, Li H, Ren CZ (2014) An investigation of workpiece temperature variation of helical milling for carbon fiber reinforced plastics (CFRP). Int J Mach Tool Manu 86:89-103. doi:10.1016/j.ijmachtools.2014.06.008

44. Zhang BY, Wang FJ, Wang XD, Li Y, Wang Q (2020) Optimized selection of process parameters based on reasonable control of axial force and hole-exit temperature in drilling of CFRP. Int J Adv Manuf Tech 110 (3-4):797-812. doi:10.1007/s00170-020-05868-9

45. Sun Y, Sun J, Li J, Xiong Q (2013) An experimental investigation of the influence of cutting parameters on cutting temperature in milling Ti6Al4V by applying semi-artificial thermocouple. Int J Adv Manuf Tech 70 (5-8):765-773. doi:10.1007/s00170-013-5294-1

46. Sheng J, Chiu Y-J, Lin B-J (2017) Determination of a coupling equation for milling parameters based on optimal cutting temperature. Int J Adv Manuf Tech 98 (1-4):129-141. doi:10.1007/s00170-017-0542-4

47. Shah D, Bhavsar S (2020) Effect of Tool Nose Radius and Machining Parameters on Cutting Force, Cutting Temperature and Surface Roughness – An Experimental Study of Ti-6Al-4V (ELI). Mater Today Proc 22:1977-1986. doi:10.1016/j.matpr.2020.03.163

48. Wang H, Sun J, Li J, Lu L, Li N (2015) Evaluation of cutting force and cutting temperature in milling carbon fiber-reinforced polymer composites. Int J Adv Manuf Tech 82 (9-12):1517-1525. doi:10.1007/s00170-015-7479-2

49. Ha SJ, Kim KB, Yang JK, Cho MW (2017) Influence of cutting temperature on carbon fiber-reinforced plastic composites in high-speed machining. J Mech Sci Technol 31 (4):1861-1867. doi:10.1007/s12206-017-0333-8

50. Rajesh N, Yohan M, Venkataramaiah P, Vani pallavi M (2017) Optimization of Cutting Parameters for Minimization of Cutting Temperature and Surface Roughness in Turning of Al6061 Alloy. Mater Today Proc 4 (8):8624-8632. doi:10.1016/j.matpr.2017.07.210

51. Weinert K, Brinkel F, Kempmann C, Pantke K (2007) The dependency of material properties and process conditions on the cutting temperatures when drilling polymers. Prod Eng 1 (4):381-387. doi:10.1007/s11740-007-0015-y

52. Guimarães B, Fernandes CM, Figueiredo D, Cerqueira MF, Carvalho O, Silva FS, Miranda G (2020) A novel approach to reduce in-service temperature in WC-Co cutting tools. Ceram Int 46 (3):3002-3008. doi:10.1016/j.ceramint.2019.09.299

53. Behera GC, Thrinadh J, Datta S (2020) Influence of cutting insert (uncoated and coated carbide) on cutting force, tool-tip temperature, and chip morphology during dry machining of Inconel 825. Mater Today Proc. doi:10.1016/j.matpr.2020.08.332

54. Sasahara H, Satake K, Takahashi W, Goto M, Yamamoto H (2017) The effect of oil mist supply on cutting point temperature and tool wear in driven rotary cutting. Prec Eng 48:158-163. doi:10.1016/j.precisioneng.2016.11.016

55. Song KH, Lim DW, Park JY, Ha SJ, Yoon GS (2020) Investigation on influence of hybrid nozzle of CryoMQL on tool wear, cutting force, and cutting temperature in milling of titanium alloys. Int J Adv Manuf Tech 110 (7-8):2093-2103. doi:10.1007/s00170-020-05646-7

56. Merino-Perez JL, Royer R, Merson E, Lockwood A, Ayvar-Soberanis S, Marshall MB (2016) Influence of workpiece constituents and cutting speed on the cutting forces developed in the conventional drilling of CFRP composites. Compos Struct 140:621-629. doi:10.1016/j.compstruct.2016.01.008

57. Yashiro T, Ogawa T, Sasahara H (2013) Temperature measurement of cutting tool and machined surface layer in milling of CFRP. Int J Mach Tool Manu 70:63-69. doi:10.1016/j.ijmachtools.2013.03.009

58. Chen T, Ye ML, Deng Y, Liu SL (2018) Study of temperature field for UVAG of CFRP based on FBG. Int J Adv Manuf Tech 96 (1-4):765-773. doi:10.1007/s00170-018-1642-5

59. Kong L, Gao D, Lu Y, Jiang Z (2020) Novel orbital drilling and reaming tool for machining holes in carbon fiber–reinforced plastic (CFRP) composite laminates. Int J Adv Manuf Tech 110 (3-4):977-988. doi:10.1007/s00170-020-05928-0

60. Zhirong L (2017) Research on bone cutting and a novel tool development. Dissertation, Harbin Institute of Technology

61. Shaw MC, Cookson JO (1985) Metal Cutting Principles. Tribol Int 18 (1):55-55

62. Budak E, Altintas Y, Armarego EJA (1996) Prediction of milling force coefficients from orthogonal cutting data. J Manuf Sci E-T Asme 118 (2):216-224. doi:Doi 10.1115/1.2831014

63. Denkena N, Rehe, & Dege. (2011) Process Force Prediction in Orbital Drilling of TiAl6V4. 9th Int Conf Adv Manuf Sys Tech

64. Wang MH, Gao L, Zheng YH (2014) An examination of the fundamental mechanics of cutting force coefficients. Int J Mach Tool Manu 78:1-7. doi:10.1016/j.ijmachtools.2013.10.008

65. Haiyan W, Xuda Q (2015) A mechanistic model for cutting force in helical milling of carbon fiber-reinforced polymers. Int J Adv Manuf Tech 82 (9-12):1485-1494. doi:10.1007/s00170-015-7460-0

Figures

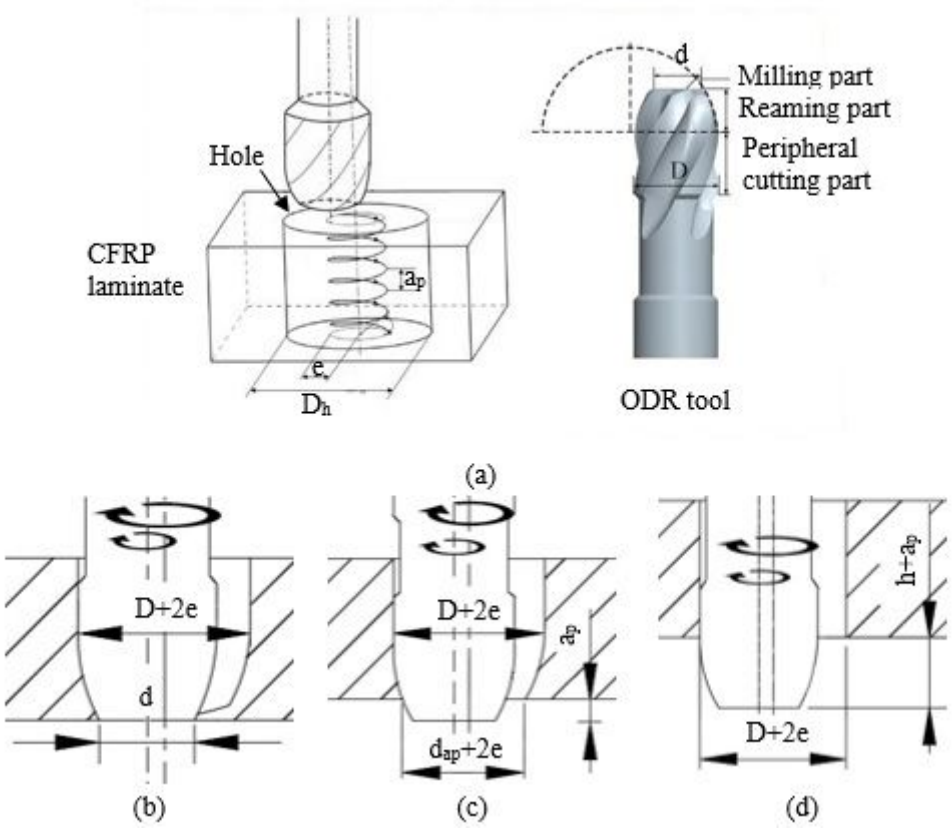

Figure 1

ODR tool and the hole processing with ODR tool: (a) ODR tool, (b)-(d) exit formation of ODR tool

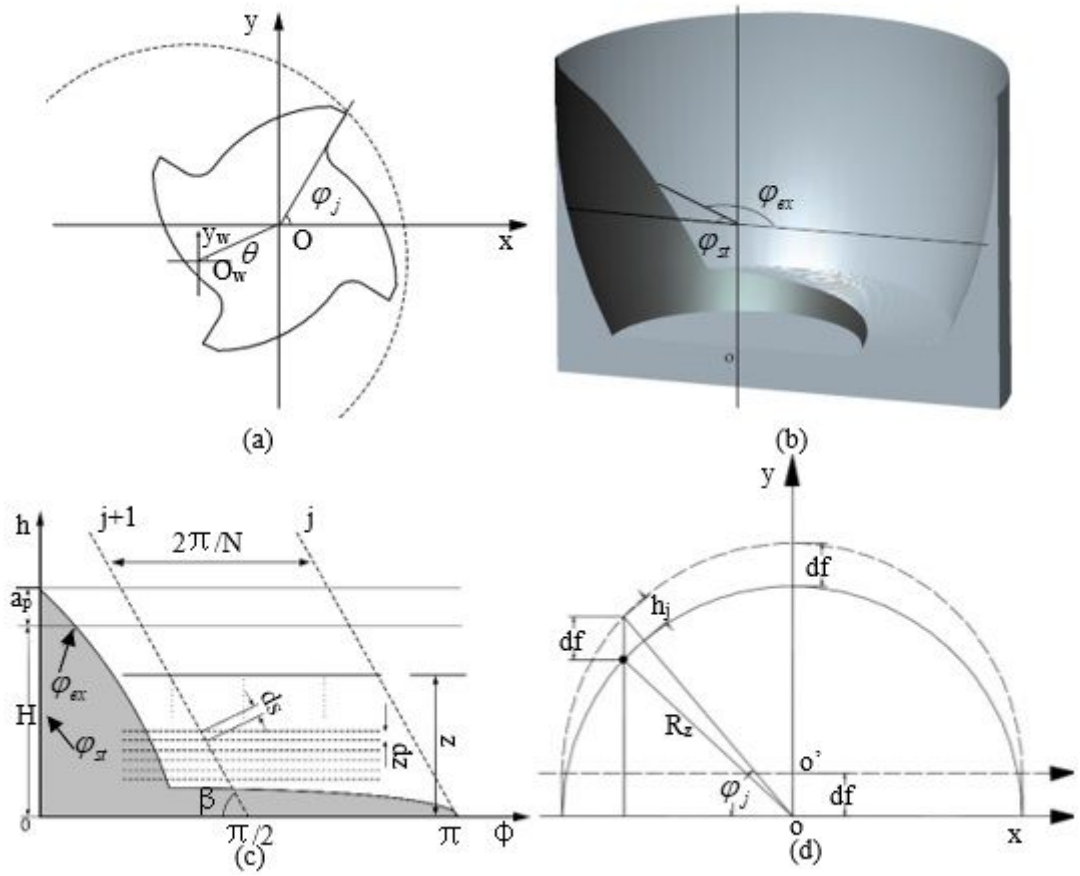

Figure 2

Illustration of the orbital drilling with ODR tool: (a) tool coordinate and workpiece coordinate, (b) undeformed chip geometry in orbital drilling with ODR tool, (c) illustration of the cutting element, (d) undeformed chip thickness

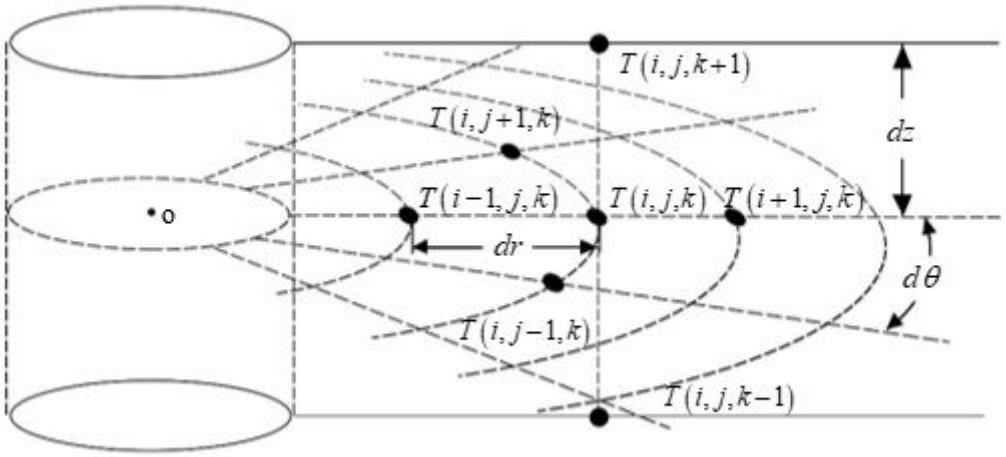

Figure 3

Diagram of the workpiece meshing

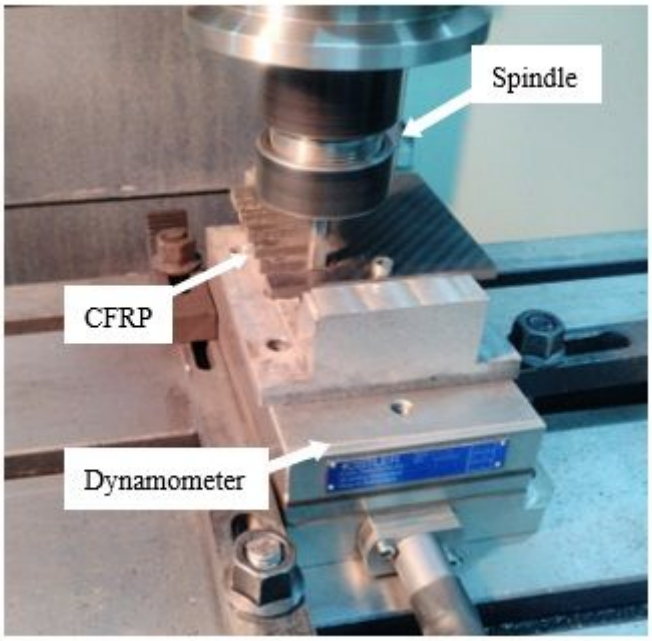

Figure 4

The experimental setup in cutting force coefficient identification experiment

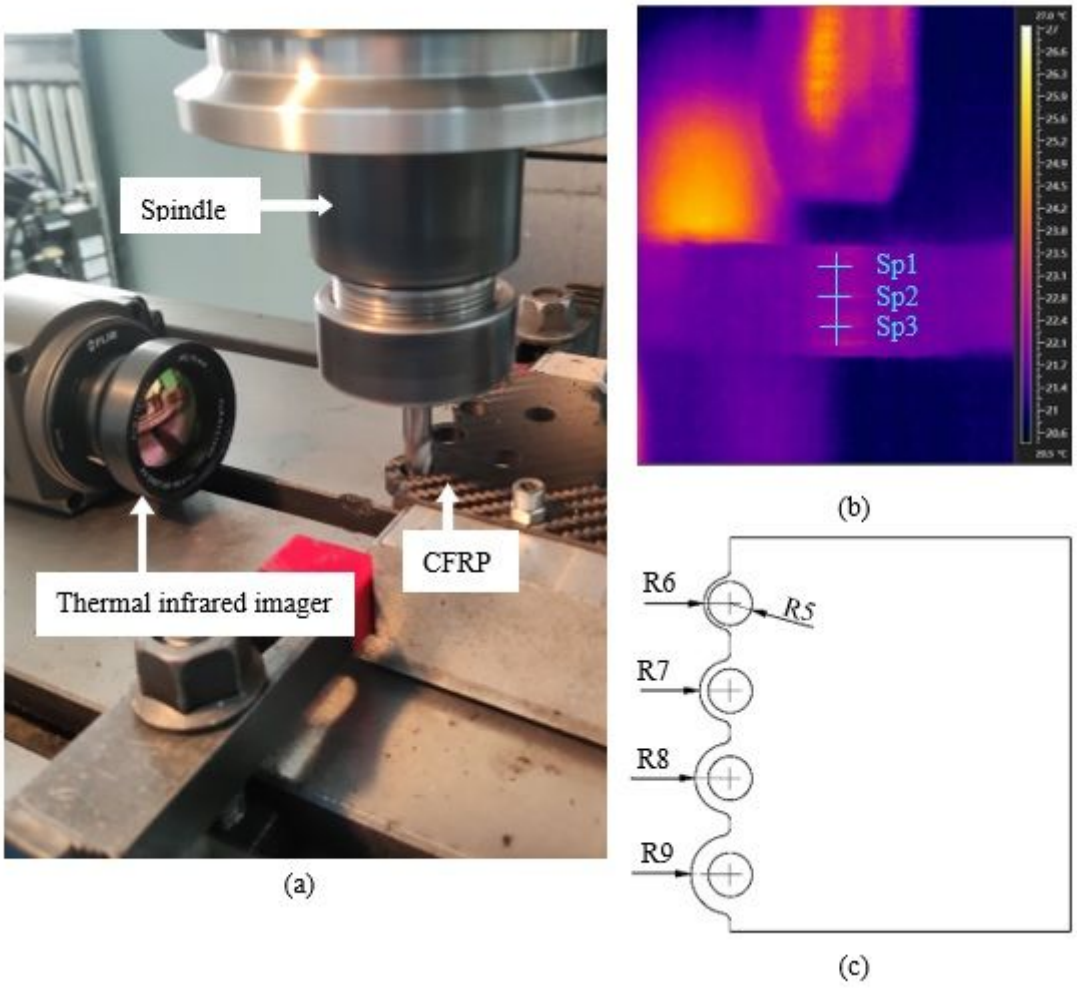

Figure 5

(a) Experimental setup in test 2 and (b) infrared image of the workpiece (c) the workpiece in verification experiment of temperature distribute model

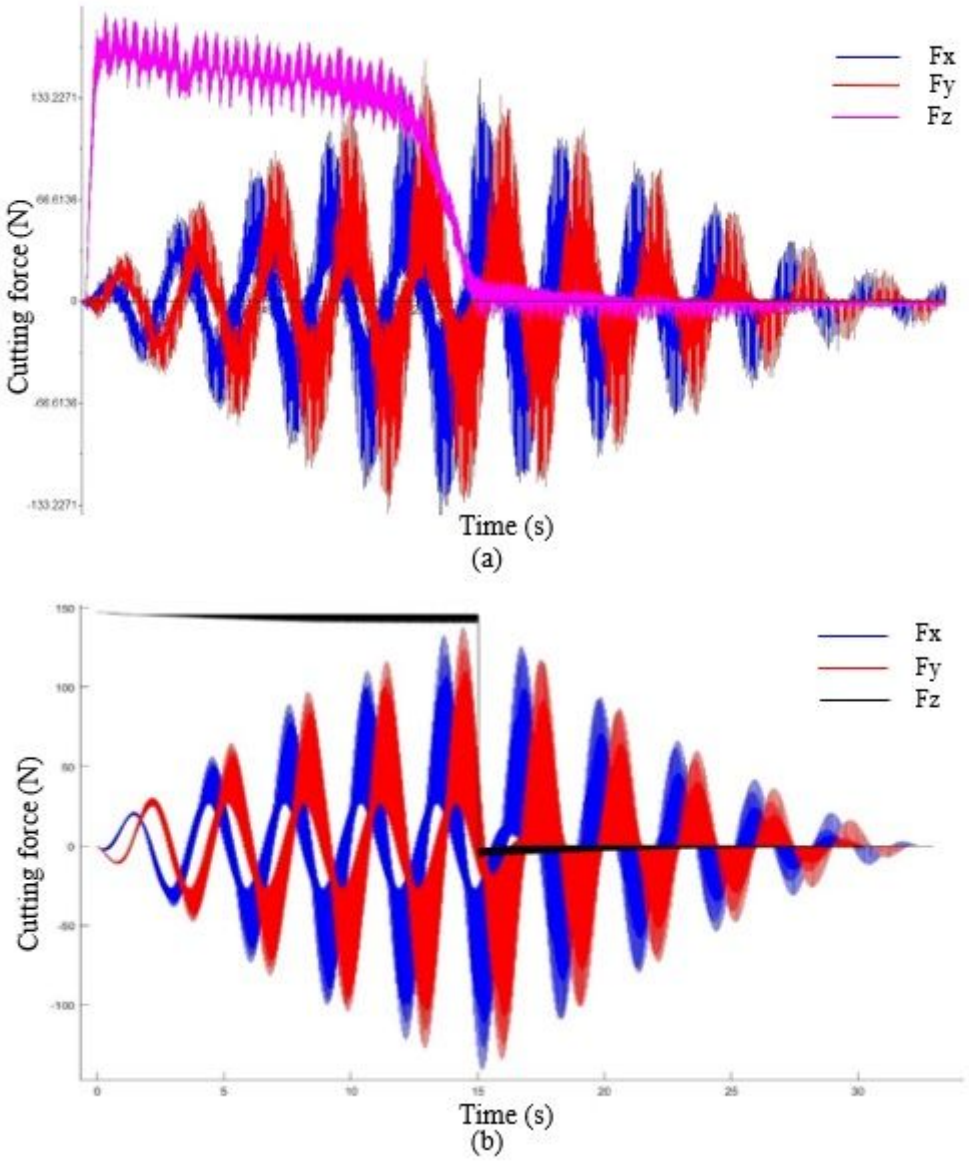

Figure 6

Prediction and experimental result: (a) experimental result, (b) prediction of cutting force model/

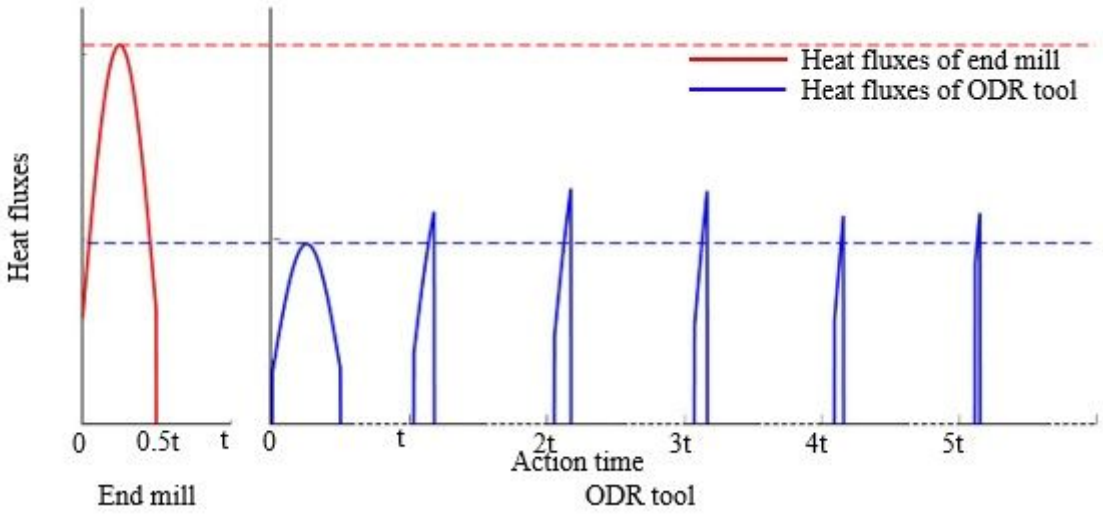

Figure 7

Heat fluxes of the peripheral cutting edge and the edge on the reaming part of two kinds of tools

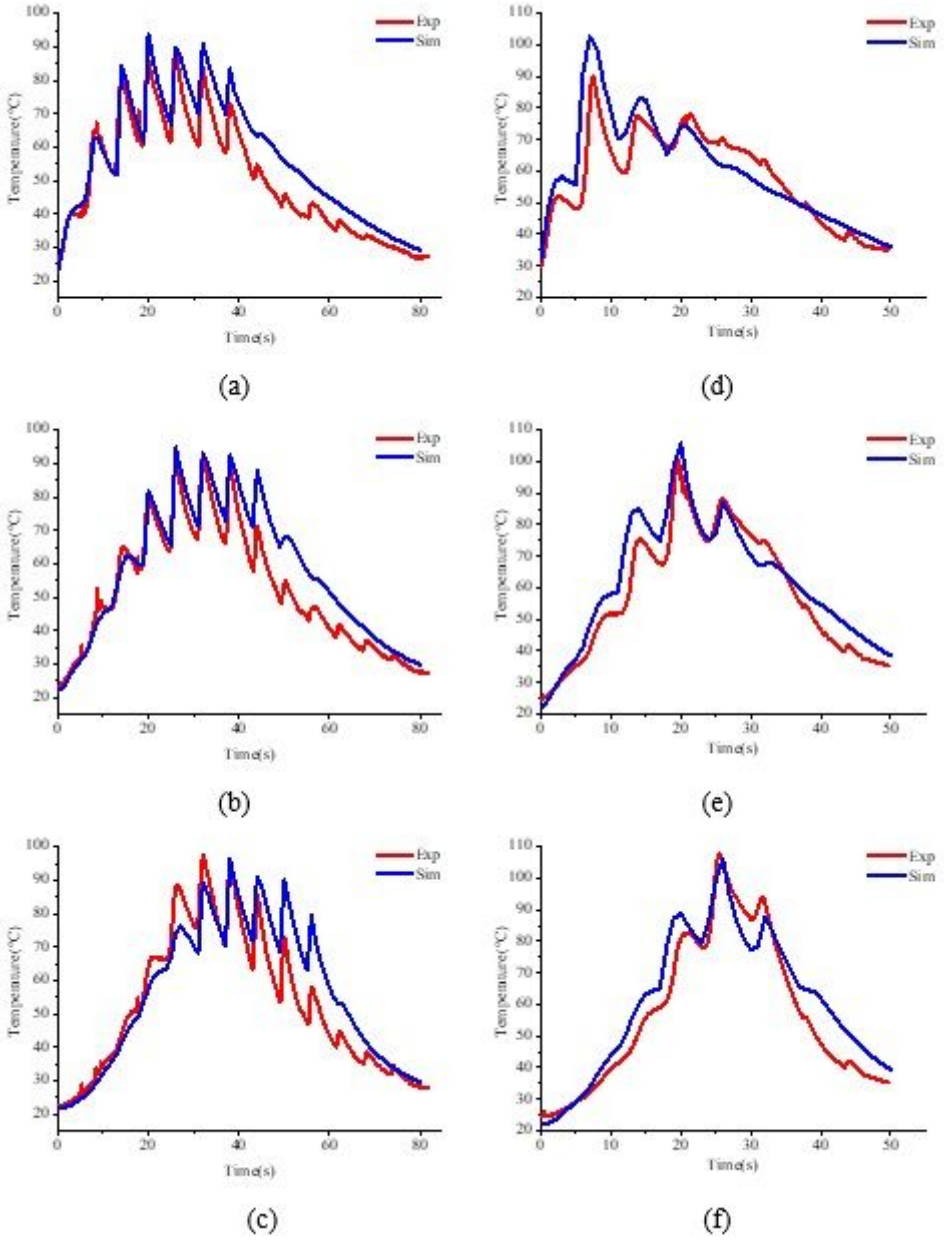

Figure 8

Comparison of simulation results and experimental results of machining temperature: (a) results comparison of ODR at sp1, (b) results comparison of ODR at sp2, (c) results comparison of ODR at sp3, (d) results comparison of end mill at sp1,(e) results comparison of end mill at sp2,(f) results comparison of end mill at sp3,

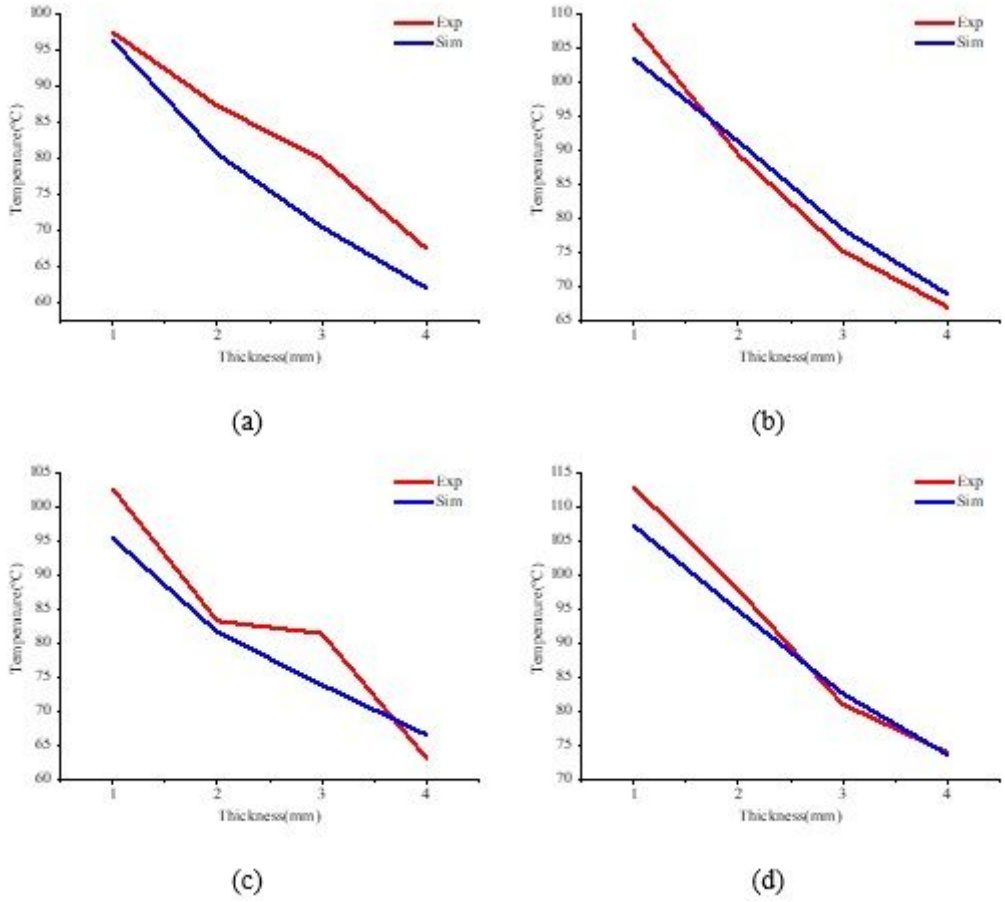

Figure 9

Maximum processing temperature of experimental results and simulation results: (a) results of ODR tool in cutting condition □, (b) results of end mill in cutting condition □, (c) results of ODR tool in cutting condition □□, (d) results of end mill in cutting condition □□